

A low-rank solver for conforming multipatch Isogeometric Analysis

Monica Montardini^{a,b,*}, Giancarlo Sangalli^{a,b}, Mattia Tani^{a,b}

^a*Dipartimento di Matematica "F. Casorati", Università di Pavia, Via A. Ferrata, 5, 27100 Pavia, Italy.*

^b*Istituto di Matematica Applicata e Tecnologie Informatiche, "E. Magenes" del CNR, Via A. Ferrata, 1, 27100 Pavia, Italy.*

Abstract

In this paper, we propose an innovative isogeometric low-rank solver for the linear elasticity model problem, specifically designed to allow multipatch domains. Our approach splits the domain into subdomains, each formed by the union of neighboring patches. Within each subdomain, we employ Tucker low-rank matrices and vectors to approximate the system matrices and right-hand side vectors, respectively. This enables the construction of local approximate fast solvers. These local solvers are then combined into an overlapping Schwarz preconditioner, which is utilized in a truncated preconditioned conjugate gradient method. Numerical experiments demonstrate the significant memory storage benefits and a uniformly bounded number of iterations with respect to both mesh size and spline degree.

Keywords: Isogeometric Analysis, truncated preconditioned conjugate gradient method, low-rank Tucker tensors, conforming multipatch

1. Introduction

Isogeometric Analysis (IgA) has undergone significant development since the seminal paper [14]. Among other reasons, IgA is interesting as high-order PDEs solver. Indeed, IgA benefits from the approximation properties of splines, which, especially in the case of maximal regularity (splines of polynomial degree p and continuity C^{p-1}) exhibits approximation properties superior to those of classical C^0 or discontinuous piecewise polynomials (see for example [2]). These approximation properties are very close to optimality in the sense of n -widths (see [10]).

As with all high-order numerical methods, having efficient solvers is fundamental, and this has been a topic of research activity in the IgA community. Among the various solutions developed in this regard, low-rank compression techniques have been recently explored, leveraging the tensorial construction of isogeometric spaces at the level of each patch. See, for example, [20, 13, 16, 24], where the authors use a low-rank representation of the isogeometric Galerkin matrices. Low-rank tensor methods have been also exploited in the solution of IgA linear systems in [12, 21], based on the Tucker format, and in [3], that uses the tensor-trains approximation of the unknown. In these papers, a single tensorial patch is considered.

In this work, we also consider tensorial patches, but in the multipatch case. This extension is not trivial since the multipatch setting is not globally tensorial. To circumvent this issue, instead of representing the unknown in the usual multipatch basis (obtained by a continuous gluing of the individual patch bases) we construct appropriate tensorial subdomains by pairing patches two by two, and represent the global unknown as the disjoint union of the unknowns of the subdomains. This representation is not unique, leading to a larger and singular linear system. However, the advantage is that, on each subdomain, we can use a solver that leverages tensorial properties, and construct then a block diagonal preconditioner for the global system. This is equivalent, in the full-rank case, to an overlapping Schwarz preconditioner for the

*Corresponding author

Email addresses: monica.montardini@unipv.it (Monica Montardini), giancarlo.sangalli@unipv.it (Giancarlo Sangalli), mattia.tani@unipv.it (Mattia Tani)

system written in the standard basis, see [1]. An additional benefit is that the global unknown admits an approximation obtained from local low-rank approximations on the subdomains. This allows us to use the low-rank preconditioner from [21] on each subdomain. We then apply a truncated preconditioned conjugate gradient solver to our singular linear system.

It is known that Krylov solvers perform well with singular systems, provided that the right-hand side lies in the range of the system matrix, see e.g. [17, 15, 25]. However, in our approach, low-rank compression is performed at each step, meaning that the iterates are not computed exactly: in this context, convergence is less understood. We also observe that truncated Krylov methods have only been introduced recently, and their theory is still under development, even for non-singular systems, see [18, 23, 27]. Although there are gaps in the mathematical understanding and therefore the convergence of the linear solver we use in this work is not guaranteed, our benchmarks show that the proposed method works well, similarly to the single-patch non-singular case considered in [21], and it delivers significant memory compression, up to two orders of magnitude compared to the full-rank case.

We mention the preprint [4], which shares with the present paper the goal of tackling multipatch isogeometric problems by combining low-rank techniques with a domain decomposition approach. However, the approach presented in [4] is different from ours both in the choice of the tensor format (tensor trains), and in the domain decomposition paradigm (non-overlapping).

The paper is organized as follows. In Section 2 we present the basics of IgA and of tensor calculus. The core of the paper is Section 3, where we propose the novel multipatch low-rank strategy. We present some numerical experiments in Section 4 while in the last section we draw some conclusions.

2. Preliminaries

2.1. B-Splines

Let m and p be two positive integers. Then, a knot vector in $[0, 1]$ is a set of non-decreasing points $\Xi := \{\xi_1, \dots, \xi_{m+p+1}\}$. We consider only open knot vectors, i.e. we set $\xi_1 = \dots = \xi_{p+1} = 0$ and $\xi_{m+1} = \dots = \xi_{m+p+1} = 1$. Besides the first and the last ones, knots can be repeated up to multiplicity p .

Univariate B-splines are piecewise polynomials $\widehat{b}_i : [0, 1] \rightarrow \mathbb{R}$ for $i = 1, \dots, m$ of degree p that can be defined from the knot vector Ξ according to Cox-De Boor recursion formulas [6]. We define the mesh-size $h := \max\{|\xi_{i+1} - \xi_i| \mid i = 1, \dots, m+p\}$ and we denote the univariate spline space as

$$\widehat{\mathcal{S}}_h^p := \text{span}\{\widehat{b}_i \mid i = 1, \dots, m\}.$$

For B-splines properties, we refer to [5]. Multivariate B-splines are defined by tensor product of univariate B-splines. In this paper we focus on three-dimensional problems. Thus, given m_d and p_d positive integers, we introduce for $d = 1, 2, 3$ the open knot vectors $\Xi_d := \{\xi_{1,d}, \dots, \xi_{m_d+p_d+1,d}\}$, the corresponding B-splines \widehat{b}_{d,i_d} , $i_d = 1, \dots, m_d$, mesh-sizes h_d and univariate spline spaces $\widehat{\mathcal{S}}_{h_d}^p$. The maximum of the mesh-sizes is denoted as $h := \max\{h_d \mid d = 1, 2, 3\}$. Note that for simplicity we are assuming that all univariate B-splines have the same degree. Multivariate B-splines $\widehat{B}_i : [0, 1]^3 \rightarrow \mathbb{R}$ are defined as

$$\widehat{B}_i(\underline{\xi}) := \widehat{b}_{1,i_1}(\xi_1)\widehat{b}_{2,i_2}(\xi_2)\widehat{b}_{3,i_3}(\xi_3),$$

where $i := (i_1, i_2, i_3)$ is a multi-index and $\underline{\xi} = (\xi_1, \xi_2, \xi_3)$. We define the corresponding spline space as

$$\widehat{\mathcal{S}}_h^p := \text{span}\left\{\widehat{B}_i \mid \text{where } i := (i_1, i_2, i_3) \text{ and } i_d = 1, \dots, m_d \text{ for } l = 1, 2, 3\right\} = \widehat{\mathcal{S}}_{h_1}^p \otimes \widehat{\mathcal{S}}_{h_2}^p \otimes \widehat{\mathcal{S}}_{h_3}^p.$$

2.2. Isogeometric spaces on a multipatch domain

Let $\Omega \subset \mathbb{R}^3$ represent the computational domain, and we assume that it can be written as the union of \mathcal{N}_{ptc} non-overlapping closed sets, called patches, i.e.

$$\Omega = \bigcup_{i=1}^{\mathcal{N}_{ptc}} \Omega^{(i)}$$

and $\Omega^{(i)} \cap \Omega^{(j)}$ has empty interior for $i \neq j$. Let $\Gamma := \left(\bigcup_{i=1}^{\mathcal{N}_{ptc}} \partial\Omega^{(i)} \right) \setminus \partial\Omega$ denote the union of patch interfaces.

For a fixed $i \in \{1, \dots, \mathcal{N}_{ptc}\}$, we introduce three positive integers $m_1^{(i)}, m_2^{(i)}, m_3^{(i)}$ and three open knot vectors $\Xi_d^{(i)} := \{\xi_{1,d}^{(i)}, \dots, \xi_{m_d^{(i)}+p+1,d}^{(i)}\}$, for $d = 1, 2, 3$, where p is another positive integer which does not depend on i and d . Let $h_d^{(i)}$ denote the mesh-size of $\Xi_d^{(i)}$ for $d = 1, 2, 3$. Moreover, we introduce $h := \max\{h_d^{(j)} \mid j = 1, \dots, \mathcal{N}_{ptc}, d = 1, 2, 3\}$. The multivariate spline space associated to each patch is denoted as $\widehat{\mathcal{S}}_{ptc}^{(i)}$. We assume that for each patch $\Omega^{(i)}$ there exists a non-singular parametrization $\mathcal{F}_i \in \left[\widehat{\mathcal{S}}_{ptc}^{(i)} \right]^3$ whose image is $\Omega^{(i)}$, i.e. $\Omega^{(i)} = \mathcal{F}_i([0, 1]^3)$ and the Jacobian matrix $J_{\mathcal{F}_i}$ is invertible everywhere. A face of a given patch $\Omega^{(i)}$ is the image through \mathcal{F}_i of a face of the unit cube. Similarly, an edge of $\Omega^{(i)}$ is the image through \mathcal{F}_i of an edge of the unit cube.

Let $\partial\Omega_D \subseteq \partial\Omega$, which will represent the portion of $\partial\Omega$ endowed with Dirichlet boundary conditions. We need the following assumption.

Assumption 1. *We assume that $\partial\Omega_D \cap \partial\Omega^{(i)}$ is either an empty set or an entire face of $\Omega^{(i)}$ for $i = 1, \dots, \mathcal{N}_{ptc}$.*

For $i = 1, \dots, \mathcal{N}_{ptc}$, we define $\widehat{\mathcal{S}}_{ptc,0}^{(i)} \subset \widehat{\mathcal{S}}_{ptc}^{(i)}$ as the space generated by the basis functions of $\widehat{\mathcal{S}}_{ptc}^{(i)}$ whose image through \mathcal{F}_i vanishes on $\partial\Omega_D$. Thanks to Assumption 1, $\widehat{\mathcal{S}}_{ptc,0}^{(i)}$ is a tensor product space, i.e.

$$\widehat{\mathcal{S}}_{ptc,0}^{(i)} := \widehat{\mathcal{S}}_{ptc,1}^{(i)} \otimes \widehat{\mathcal{S}}_{ptc,2}^{(i)} \otimes \widehat{\mathcal{S}}_{ptc,3}^{(i)},$$

where $\widehat{\mathcal{S}}_{ptc,d}^{(i)} := \text{span} \left\{ \widehat{b}_{d,j}^{(i)} \mid j = 1, \dots, n_{ptc,d}^{(i)} \right\}$ are univariate spline spaces, with $n_{ptc,d}^{(i)} := \dim \left(\widehat{\mathcal{S}}_{ptc,d}^{(i)} \right)$, for $d = 1, 2, 3$.

Following the isoparametric concept, we define the local isogeometric space on the i -th patch as

$$V_{ptc}^{(i)} := \left\{ \hat{v}_h \circ \mathcal{F}_i^{-1} \mid \hat{v}_h \in \widehat{\mathcal{S}}_{ptc,0}^{(i)} \right\}.$$

Note that $\dim \left(V_{ptc}^{(i)} \right) = \prod_{d=1}^3 n_{ptc,d}^{(i)} =: n_{ptc}^{(i)}$. Moreover, the isogeometric space over Ω is defined as

$$V_h := \left\{ v \in H^1(\Omega) \mid v|_{\Omega^{(i)}} \in V_{ptc}^{(i)}, i = 1, \dots, \mathcal{N}_{ptc} \right\}. \quad (2.1)$$

Throughout the paper, we make the following assumption on the meshes.

Assumption 2. *We assume that the meshes are conforming at the patch interfaces, i.e. for all i and j such that $\partial\Omega^{(i)} \cap \partial\Omega^{(j)} \neq \emptyset$ and the intersection is not a point, the interfaces are fully matching (see [14] for more details).*

Under this assumption, we collect all the basis functions from all local spaces, and then identify those functions whose restriction to the interface Γ assumes the same values and it is not identically zero. The resulting set of functions forms a basis for V_h .

2.3. Model problem

Our model problem is the compressible linear elasticity problem. Let $\partial\Omega = \partial\Omega_D \cup \partial\Omega_N$ with $\partial\Omega_D \cap \partial\Omega_N = \emptyset$ and where $\partial\Omega_D$ is non-empty and satisfies Assumption 1. Let $H_D^1(\Omega) := \{v \in H^1(\Omega) \mid v = 0 \text{ on } \partial\Omega_D\}$. For simplicity, we consider only homogeneous Dirichlet boundary conditions, but the non-homogeneous case can be treated similarly. Then, given $\underline{f} \in [L^2(\Omega)]^3$ and $\underline{g} \in [L^2(\partial\Omega_N)]^3$, we consider the Galerkin problem: find $\underline{u} \in [H_D^1(\Omega)]^3$ such that for all $\underline{v} \in [H_D^1(\Omega)]^3$

$$a(\underline{u}, \underline{v}) = F(\underline{v}),$$

where we define

$$a(\underline{u}, \underline{v}) := 2\mu \int_{\Omega} \varepsilon(\underline{u}) : \varepsilon(\underline{v}) d\underline{x} + \lambda \int_{\Omega} (\nabla \cdot \underline{u}) (\nabla \cdot \underline{v}) d\underline{x}, \quad (2.2)$$

$$F(\underline{v}) := \int_{\Omega} \underline{f} \cdot \underline{v} d\underline{x} + \int_{\partial\Omega_N} \underline{g} \cdot \underline{v} ds, \quad (2.3)$$

$\varepsilon(\underline{v}) := \frac{1}{2} (\nabla \underline{v} + (\nabla \underline{v})^T)$ is the symmetric gradient, while λ and μ denote the material Lamé coefficients, that for simplicity we assume to be constant and positive and such that the Poisson ratio $\frac{\lambda}{2(\mu+\lambda)}$ is smaller than 0.5.

The corresponding discrete Galerkin problem that we want to solve is the following: find $\underline{u}_h \in [V_h]^3$ such that

$$a(\underline{u}_h, \underline{v}_h) = F(\underline{v}_h), \quad \text{for all } \underline{v}_h \in [V_h]^3, \quad (2.4)$$

where the space V_h has been defined in (2.1). Note that $[V_h]^3 \subseteq [H_D^1(\Omega)]^3$.

2.4. The Tucker format

Throughout the paper, the entries of a matrix $\mathbf{B} \in \mathbb{R}^{m_1 \times m_2}$ are denoted with $[\mathbf{B}]_{i,j}$, $i = 1, \dots, m_1$, $j = 1, \dots, m_2$. Similarly, the entries of a tensor $\mathfrak{B} \in \mathbb{R}^{m_1 \times m_2 \times m_3}$ are denoted with $[\mathfrak{B}]_{i,j,k}$, $i = 1, \dots, m_1$, $j = 1, \dots, m_2$, $k = 1, \dots, m_3$.

Given $\mathbf{B} \in \mathbb{R}^{m_1 \times m_2}$ and $\mathbf{C} \in \mathbb{R}^{n_1 \times n_2}$, their Kronecker product is defined as

$$\mathbf{B} \otimes \mathbf{C} = \begin{bmatrix} [\mathbf{B}]_{1,1} \mathbf{C} & \dots & [\mathbf{B}]_{1,m_2} \mathbf{C} \\ \vdots & \ddots & \vdots \\ [\mathbf{B}]_{m_1,1} \mathbf{C} & \dots & [\mathbf{B}]_{m_1,m_2} \mathbf{C} \end{bmatrix} \in \mathbb{R}^{m_1 n_1 \times m_2 n_2}.$$

The notion of Kronecker product can be generalized to tensors of higher dimensions. In particular, given $\mathfrak{B} \in \mathbb{R}^{m_1 \times m_2 \times m_3}$ and $\mathfrak{C} \in \mathbb{R}^{n_1 \times n_2 \times n_3}$, their Kronecker product is the tensor of $\mathbb{R}^{m_1 n_1 \times m_2 n_2 \times m_3 n_3}$ whose entries are

$$[\mathfrak{B} \otimes \mathfrak{C}]_{k_1, k_2, k_3} = [\mathfrak{B}]_{i_1, i_2, i_3} [\mathfrak{C}]_{j_1, j_2, j_3} \quad \text{with} \quad k_d = j_d + (i_d - 1)n_d \quad \text{for} \quad d = 1, 2, 3.$$

In this paper we adopt the notation of [22] and say that a vector $\mathbf{v} \in \mathbb{R}^{n_1 n_2 n_3}$ is in Tucker format (or that it is a Tucker vector) when it is written as

$$\mathbf{v} = \sum_{r_3=1}^{R_3^v} \sum_{r_2=1}^{R_2^v} \sum_{r_1=1}^{R_1^v} [\mathfrak{v}]_{r_1, r_2, r_3} v_{(3, r_3)} \otimes v_{(2, r_2)} \otimes v_{(1, r_1)}, \quad (2.5)$$

where $v_{(d, r_d)} \in \mathbb{R}^{n_d}$ for $d = 1, 2, 3$ and $r_d = 1, \dots, R_d^v$, while $\mathfrak{v} \in \mathbb{R}^{R_1^v \times R_2^v \times R_3^v}$ is called the core tensor of \mathbf{v} . Here the triplet (R_1^v, R_2^v, R_3^v) is referred to as the multilinear rank of \mathbf{v} . Note that $\mathbf{v} \in \mathbb{R}^{n_1 n_2 n_3}$, and the memory required to store it as a Tucker vector is $R_1^v n_1 + R_2^v n_2 + R_3^v n_3$. This can be significantly lower than the standard $n_1 n_2 n_3$, provided that $R_d^v \ll n_d$, for $d = 1, 2, 3$.

Similarly, we say that a matrix $\mathbf{B} \in \mathbb{R}^{m_1 m_2 m_3 \times n_1 n_2 n_3}$ is in Tucker format (or that it is a Tucker matrix) when it is written as

$$\mathbf{B} = \sum_{r_3=1}^{R_3^B} \sum_{r_2=1}^{R_2^B} \sum_{r_1=1}^{R_1^B} [\mathfrak{B}]_{r_1, r_2, r_3} B_{(3, r_3)} \otimes B_{(2, r_2)} \otimes B_{(1, r_1)}, \quad (2.6)$$

where $B_{(d, r_d)} \in \mathbb{R}^{m_d \times n_d}$ for $d = 1, 2, 3$, $r_d = 1, \dots, R_d^B$, and $\mathfrak{B} \in \mathbb{R}^{R_1^B \times R_2^B \times R_3^B}$.

The matrix-vector product between a Tucker matrix \mathbf{B} as in (2.6) and a Tucker vector \mathbf{v} as in (2.5) can be efficiently computed since

$$\begin{aligned}\mathbf{B}\mathbf{v} &= \sum_{r'_1, r'_2, r'_3} \sum_{r''_1, r''_2, r''_3} [\mathfrak{B}]_{r'_1, r'_2, r'_3} [\mathbf{v}]_{r''_1, r''_2, r''_3} \left(B_{(3, r'_3)} v_{(3, r''_3)} \right) \otimes \left(B_{(2, r'_2)} v_{(2, r''_2)} \right) \otimes \left(B_{(1, r'_1)} v_{(1, r''_1)} \right) \\ &= \sum_{r_3=1}^{R_3^{\mathbf{B}} R_3^{\mathbf{v}}} \sum_{r_2=1}^{R_2^{\mathbf{B}} R_2^{\mathbf{v}}} \sum_{r_1=1}^{R_1^{\mathbf{B}} R_1^{\mathbf{v}}} [\mathfrak{B} \otimes \mathfrak{C}]_{r_1, r_2, r_3} \left(B_{(3, r'_3)} v_{(3, r''_3)} \right) \otimes \left(B_{(2, r'_2)} v_{(2, r''_2)} \right) \otimes \left(B_{(1, r'_1)} v_{(1, r''_1)} \right)\end{aligned}$$

where, in the last line, r'_d and r''_d satisfy $r_d = r''_d + (r'_d - 1)n_d$, for $d = 1, 2, 3$. Note that $\mathbf{B}\mathbf{v}$ is still a Tucker vector with multilinear rank $(R_1^{\mathbf{B}} R_1^{\mathbf{v}}, R_2^{\mathbf{B}} R_2^{\mathbf{v}}, R_3^{\mathbf{B}} R_3^{\mathbf{v}})$.

Another operation where the Tucker structure can be exploited is the scalar product. Let \mathbf{v} as in (2.5) and let

$$\mathbf{w} = \sum_{r_3=1}^{R_3^{\mathbf{w}}} \sum_{r_2=1}^{R_2^{\mathbf{w}}} \sum_{r_1=1}^{R_1^{\mathbf{w}}} [\mathfrak{w}]_{r_1, r_2, r_3} w_{(3, r_3)} \otimes w_{(2, r_2)} \otimes w_{(1, r_1)}, \quad (2.7)$$

where $w_{(d, r_d)} \in \mathbb{R}^{n_d}$ for $d = 1, 2, 3$ and $r_d = 1, \dots, R_d^{\mathbf{w}}$. Then

$$\mathbf{v} \cdot \mathbf{w} = \sum_{r_3=1}^{R_3^{\mathbf{v}}} \sum_{r_2=1}^{R_2^{\mathbf{v}}} \sum_{r_1=1}^{R_1^{\mathbf{v}}} \sum_{r'_3=1}^{R_3^{\mathbf{w}}} \sum_{r'_2=1}^{R_2^{\mathbf{w}}} \sum_{r'_1=1}^{R_1^{\mathbf{w}}} [\mathbf{v}]_{r_1, r_2, r_3} [\mathfrak{w}]_{r'_1, r'_2, r'_3} \prod_{d=1}^3 v_{(d, r_d)} \cdot w_{(d, r'_d)}$$

The sum between two Tucker vectors is still a Tucker vector with multilinear rank equal to the sum of the multilinear ranks of the addends. Precisely, let \mathbf{v} as in (2.5) and \mathbf{w} as in (2.7). Then

$$\mathbf{z} = \mathbf{v} + \mathbf{w} = \sum_{r_3=1}^{R_3^{\mathbf{v}} + R_3^{\mathbf{w}}} \sum_{r_2=1}^{R_2^{\mathbf{v}} + R_2^{\mathbf{w}}} \sum_{r_1=1}^{R_1^{\mathbf{v}} + R_1^{\mathbf{w}}} \mathfrak{z}_{r_1, r_2, r_3} z_{(3, r_3)} \otimes z_{(2, r_2)} \otimes z_{(1, r_1)},$$

where

$$z_{(d, r_d)} = \begin{cases} v_{(d, r_d)} & \text{for } r_d = 1, \dots, R_d^{\mathbf{v}} \\ w_{(d, r_d - R_d^{\mathbf{v}})} & \text{for } r_d = R_d^{\mathbf{v}} + 1, \dots, R_d^{\mathbf{v}} + R_d^{\mathbf{w}} \end{cases}, \quad d = 1, 2, 3,$$

and where the core tensor \mathfrak{z} is a block diagonal tensor defined by concatenating the core tensors of \mathbf{v} and \mathbf{w} .

3. Low-rank multipatch method

We introduce another subdivision of the computational domain, namely

$$\Omega = \bigcup_{i=1}^{\mathcal{N}_{sub}} \Theta^{(i)}.$$

Here, differently from the patches defined in Section 2.2, the subdomains $\Theta^{(j)}$ are allowed to overlap, i.e. the intersection of two different subdomains can have a non-empty interior.

We denote with $V_{sub}^{(i)}$ the subspace of V_h whose functions vanish outside $\Theta^{(i)}$, i.e.

$$V_{sub}^{(i)} = \left\{ v_h \in V_h \mid v_h = 0 \text{ on } \Omega \setminus \Theta^{(i)} \right\}.$$

As a basis for $V_{sub}^{(i)}$, we choose the set of basis functions of V_h whose support is included in $\Theta^{(i)}$. A crucial assumption is that each space $V_{sub}^{(i)}$ can be written as (the pushforward of) a tensor product spline space. Precisely, we make the following assumption.

Assumption 3. We assume that

$$V_{sub}^{(i)} = \left\{ \hat{v}_h \circ \mathcal{G}_i^{-1} \mid \hat{v}_h \in \widehat{\mathcal{S}}_{sub,0}^{(i)} \right\}, \quad (3.1)$$

where $\mathcal{G}_i : [0, 1]^3 \rightarrow \Theta^{(i)}$ is a non-singular and differentiable map, while

$$\widehat{\mathcal{S}}_{sub,0}^{(i)} = \widehat{\mathcal{S}}_{sub,1}^{(i)} \otimes \widehat{\mathcal{S}}_{sub,2}^{(i)} \otimes \widehat{\mathcal{S}}_{sub,3}^{(i)} \quad (3.2)$$

is a tensor product spline space.

Here $\widehat{\mathcal{S}}_{sub,d}^{(i)}$, $d = 1, 2, 3$, represent univariate spline spaces, whose dimension is denoted with $n_{sub,d}^{(i)}$. Note that $\dim(V_{sub}^{(i)}) = \prod_{d=1}^3 n_{sub,d}^{(i)} =: n_{sub}^{(i)}$.

In the setting described in Section 2.2, the subdomains $\Theta^{(i)}$ and the corresponding spaces $V_{sub}^{(i)}$ satisfying (3.1) can be obtained by merging pairs of isogeometric patches and the corresponding spaces. We give details for this construction in Section 3.4.

3.1. The linear system

We split the solution $\underline{u}_h \in [V_h]^3$ of the Galerkin problem (2.4) as

$$\underline{u}_h = \sum_j^{\mathcal{N}_{sub}} \underline{u}_h^{(j)}, \quad \underline{u}_h^{(j)} \in [V_{sub}^{(j)}]^3. \quad (3.3)$$

The functions $\underline{u}_h^{(1)}, \dots, \underline{u}_h^{(\mathcal{N}_{sub})}$ represent the unknowns. Due to the overlap between the subdomains, the subspaces $[V_{sub}^{(1)}]^3, \dots, [V_{sub}^{(\mathcal{N}_{sub})}]^3$ are not necessarily in direct sum. As a result, $\underline{u}_h^{(1)}, \dots, \underline{u}_h^{(\mathcal{N}_{sub})}$ are not uniquely determined in general. Instead, they are selected by the Krylov iterative solver, based on the initial iterate, without the need to impose any average condition.

In order to set up the linear system, we consider the same splitting for the test functions, and on each space $[V_{sub}^{(j)}]^3$ we choose as basis the set

$$\left\{ \underline{e}_k B_i^{(j)} \mid B_i^{(j)} \text{ basis function for } V_{sub}^{(j)}, k = 1, 2, 3 \right\},$$

where \underline{e}_k is the k -th vector of the canonical basis of \mathbb{R}^3 , $k = 1, 2, 3$. Therefore, the solution of (2.4) can be obtained from (3.3) and the linear system:

$$\mathbf{A} \mathbf{u} = \begin{bmatrix} \mathbf{A}^{(1,1)} & \dots & \mathbf{A}^{(1,\mathcal{N}_{sub})} \\ \vdots & & \vdots \\ \mathbf{A}^{(\mathcal{N}_{sub},1)} & \dots & \mathbf{A}^{(\mathcal{N}_{sub},\mathcal{N}_{sub})} \end{bmatrix} \begin{bmatrix} \mathbf{u}^{(1)} \\ \vdots \\ \mathbf{u}^{(\mathcal{N}_{sub})} \end{bmatrix} = \begin{bmatrix} \mathbf{f}^{(1)} \\ \vdots \\ \mathbf{f}^{(\mathcal{N}_{sub})} \end{bmatrix} = \mathbf{f}, \quad (3.4)$$

where, for $i, j = 1, \dots, \mathcal{N}_{sub}$, $\mathbf{u}^{(j)}$ is the coordinate vector of $\underline{u}_h^{(j)}$, while $\mathbf{f}^{(i)} \in \mathbb{R}^{3n_{sub}^{(i)}}$ and $\mathbf{A}^{(i,j)} \in \mathbb{R}^{3n_{sub}^{(i)} \times 3n_{sub}^{(j)}}$ are respectively the vector and matrix representations of the functional (2.3) and of the bilinear form (2.2), when considering $[V_{sub}^{(i)}]^3$ as test function space and $[V_{sub}^{(j)}]^3$ as trial function space. Note that the vectorial nature of the basis functions naturally induces a further block structure in $\mathbf{A}^{(i,j)}$ and $\mathbf{f}^{(i)}$:

$$\mathbf{A}^{(i,j)} = \begin{bmatrix} \mathbf{A}^{(i,j,1,1)} & \mathbf{A}^{(i,j,1,2)} & \mathbf{A}^{(i,j,1,3)} \\ \mathbf{A}^{(i,j,2,1)} & \mathbf{A}^{(i,j,2,2)} & \mathbf{A}^{(i,j,2,3)} \\ \mathbf{A}^{(i,j,3,1)} & \mathbf{A}^{(i,j,3,2)} & \mathbf{A}^{(i,j,3,3)} \end{bmatrix}, \quad \mathbf{f}^{(i)} = \begin{bmatrix} \mathbf{f}^{(i,1)} \\ \mathbf{f}^{(i,2)} \\ \mathbf{f}^{(i,3)} \end{bmatrix},$$

with $\mathbf{A}^{(i,j,k,\ell)} \in \mathbb{R}^{n_{sub}^{(i)} \times n_{sub}^{(j)}}$ and $\mathbf{f}^{(i,k)} \in \mathbb{R}^{n_{sub}^{(i)}}$ for $k, \ell = 1, 2, 3$.

The linear system (3.4) may be singular. Nevertheless, it is solvable (as there exists a solution of the Galerkin problem) and since \mathbf{A} is symmetric and positive semidefinite one solution could be found by a conjugate gradient method, see [17].

As a further step, in the spirit of [21], we consider low-rank Tucker approximations of matrix and vector blocks, i.e.

$$\mathbf{A}^{(i,j,k,\ell)} \approx \tilde{\mathbf{A}}^{(i,j,k,\ell)} = \sum_{r_3=1}^{R_3^A} \sum_{r_2=1}^{R_2^A} \sum_{r_1=1}^{R_1^A} \mathfrak{A}_{r_1,r_2,r_3} \tilde{A}_{(3,r_3)}^{(i,j,k,\ell)} \otimes \tilde{A}_{(2,r_2)}^{(i,j,k,\ell)} \otimes \tilde{A}_{(1,r_1)}^{(i,j,k,\ell)}, \quad (3.5)$$

$$\mathbf{f}^{(i,k)} \approx \tilde{\mathbf{f}}^{(i,k)} = \sum_{r_3=1}^{R_3^f} \sum_{r_2=1}^{R_2^f} \sum_{r_1=1}^{R_1^f} \mathfrak{f}_{r_1,r_2,r_3} \tilde{f}_{(3,r_3)}^{(i,k)} \otimes f_{(2,r_2)}^{(i,k)} \otimes f_{(1,r_1)}^{(i,k)}, \quad (3.6)$$

for $i, j = 1, \dots, \mathcal{N}_{sub}$, $k, \ell = 1, 2, 3$, where $R_d^A = R_d^A(i, j, k, \ell)$ and $R_d^f = R_d^f(i, k)$ for $d = 1, 2, 3$. In Section 3.4 we give details on how these approximations can be performed, when the subdomains are defined as unions of neighboring patches. We emphasize that, for the proposed strategy to be beneficial, the multilinear ranks of the approximations, which depend on the geometry coefficients and on the forcing term, have to be reasonably small.

We collect all the newly defined matrix blocks $\tilde{\mathbf{A}}^{(i,j,k,\ell)}$ and vector blocks $\tilde{\mathbf{f}}^{(i,k)}$ into a single matrix $\tilde{\mathbf{A}}$ and a single vector $\tilde{\mathbf{f}}$, respectively. Then we look for a vector $\tilde{\mathbf{u}}$ with blocks in Tucker format that approximately solves the linear system

$$\tilde{\mathbf{A}}\tilde{\mathbf{u}} = \tilde{\mathbf{f}}.$$

Following [21], we tackle the above problem using a variant of the truncated preconditioned conjugate gradient (TPCG) method [18, 29]. This is similar to the standard preconditioned conjugate gradient, but after each step a truncation is applied to the vector blocks in order keep their ranks sufficiently small.

3.2. The preconditioner

As an “ideal” preconditioner for $\tilde{\mathbf{A}}$ we consider the block diagonal matrix

$$\mathbf{P} = \begin{bmatrix} \mathbf{P}^{(1)} & 0 & \dots & 0 \\ 0 & \mathbf{P}^{(2)} & \dots & 0 \\ \vdots & \vdots & \ddots & \vdots \\ 0 & 0 & \dots & \mathbf{P}^{(\mathcal{N}_{sub})} \end{bmatrix},$$

where for each $i = 1, \dots, \mathcal{N}_{sub}$, $\mathbf{P}^{(i)}$ is a block diagonal approximation of $\mathbf{A}^{(i,i)}$, i.e.

$$\mathbf{P}^{(i)} = \begin{bmatrix} \mathbf{P}^{(i,1)} & 0 & 0 \\ 0 & \mathbf{P}^{(i,2)} & 0 \\ 0 & 0 & \mathbf{P}^{(i,3)} \end{bmatrix},$$

where $\mathbf{P}^{(i,k)}$ is an approximation of $\mathbf{A}^{(i,i,k,k)}$, $k = 1, 2, 3$. More precisely, we choose

$$\mathbf{P}^{(i,k)} = c_1^{(i,k)} M_3^{(i)} \otimes M_2^{(i)} \otimes K_1^{(i)} + c_2^{(i,k)} M_3^{(i)} \otimes K_2^{(i)} \otimes M_1^{(i)} + c_3^{(i,k)} K_3^{(i)} \otimes M_2^{(i)} \otimes M_1^{(i)}, \quad (3.7)$$

where, for $d = 1, 2, 3$, $K_d^{(i)}$ and $M_d^{(i)}$ are respectively the stiffness and mass matrix over the univariate spline space $\hat{\mathcal{S}}_{sub,d}^{(i)}$. Differently from [21], here we introduce some constant coefficients $c_\ell^{(i,k)} \in \mathbb{R}$ that aim to take into account the geometry and the elasticity coefficients, whose choice is discussed below. We emphasize that a similar approach was used in [11].

Note that if $c_\ell^{(i,k)} = 1$ for every $\ell = 1, 2, 3$, then $\mathbf{P}^{(i,k)}$ represents the discretization of the Laplace operator over the spline space $\hat{\mathcal{S}}_{sub,0}^{(i)}$.

We recall that, as discussed in [1, Theorem 2], the use of a block diagonal preconditioner is equivalent to the use of additive overlapping Schwarz preconditioners for the nonsingular linear system obtained by constructing a global spline basis. Here, however, each diagonal block $(\mathbf{P}^{(i,k)})^{-1}$ is further approximated with a low-rank Tucker matrix following the steps described in [21, Section 4.2]. We emphasize in particular that this strategy is not spoiled by the presence of the constant coefficients. A key feature of this approach is that the action of $(\tilde{\mathbf{P}}^{(i,k)})^{-1}$ on a vector can be computed using a variant of the fast diagonalization method [19, 26] that exploits the fast Fourier transform (FFT), yielding almost linear complexity. In conclusion, the preconditioner $\tilde{\mathbf{P}}$ is the block diagonal matrix obtained by collecting all matrices $\tilde{\mathbf{P}}^{(i,k)}$, for $i = 1, \dots, \mathcal{N}_{sub}$, $k = 1, 2, 3$.

We now discuss the choice of the constant coefficients $c_\ell^{(i,k)}$ appearing in (3.7). We fix $i \in \{1, \dots, \mathcal{N}_{sub}\}$ and $k \in \{1, 2, 3\}$. Let $v_h \in V_{sub}^{(i)}$ and let \mathbf{v} denote its representing vector. It holds

$$\mathbf{v}^T \mathbf{A}^{(i,i,k,k)} \mathbf{v} = \int_{\Theta^{(i)}} 2\mu \varepsilon(\underline{e}_k v_h) : \varepsilon(\underline{e}_k v_h) + \lambda (\nabla \cdot \underline{e}_k v_h) (\nabla \cdot \underline{e}_k v_h) d\underline{x} = \int_{[0,1]^3} \left(\nabla \hat{v}_{sub}^{(i)} \right)^T Q^{(i,k)} \nabla \hat{v}_{sub}^{(i)} d\underline{\xi},$$

where $\hat{v}_{sub}^{(i)} = v_h \circ \mathcal{G}_i \in \widehat{\mathcal{S}}_{sub,0}^{(i)}$, and

$$Q^{(i,k)} = |\det(J_{\mathcal{G}_i})| J_{\mathcal{G}_i}^{-1} \left[\mu (I_3 + \underline{e}_k \underline{e}_k^T) + \lambda \underline{e}_k \underline{e}_k^T \right] J_{\mathcal{G}_i}^{-T}.$$

Here I_3 denotes the 3×3 identity matrix. Moreover,

$$\mathbf{v}^T \mathbf{P}^{(i,k)} \mathbf{v} = \int_{[0,1]^3} \left(\nabla \hat{v}_{sub}^{(i)} \right)^T \begin{bmatrix} c_1^{(i,k)} & 0 & 0 \\ 0 & c_2^{(i,k)} & 0 \\ 0 & 0 & c_3^{(i,k)} \end{bmatrix} \nabla \hat{v}_{sub}^{(i)} d\underline{\xi}.$$

It is apparent that the 3×3 constant matrix appearing in the above formula should be chosen as the best constant diagonal approximation of $Q^{(i,k)}$. It is therefore reasonable to require that

$$c_\ell^{(i,k)} \approx Q_{\ell,\ell}^{(i,k)}(\xi_1, \xi_2, \xi_3), \quad \ell = 1, 2, 3, \quad \xi_1, \xi_2, \xi_3 \in [0, 1].$$

For $\ell = 1, 2, 3$, we choose $c_\ell^{(i,k)}$ as the average of $Q_{\ell,\ell}^{(i,k)}$ evaluated on the breakpoints of the ℓ -th knot vector of the geometry that describes $\Theta^{(i)}$ and their midpoints.

3.3. The TPCG method with block-wise truncation

As already mentioned, a crucial feature of the TPCG method is the truncation step. Indeed, the operations performed during the iterative process, namely the vector sums and more importantly the matrix-vector products, increase the multilinear ranks of the iterates. Therefore, it is of paramount importance to keep their rank reasonably small through truncation. We emphasize that in our version of the TPCG method the involved vectors (and matrices) do not have a global Tucker structure. Instead, they can be subdivided into blocks with Tucker structure, each with its own multilinear rank. Therefore, all the operations that exploit the Tucker structure, including truncation, are performed to each matrix/vector block separately.

The simplest truncation operator considered here is relative truncation and it is denoted with \mathbf{T}^{rel} . Given a Tucker vector \mathbf{v} and a relative tolerance $\epsilon > 0$, $\tilde{\mathbf{v}} = \mathbf{T}^{\text{rel}}(\mathbf{v}, \eta)$ is a Tucker vector with smaller or equal multilinear rank (in each direction) such that

$$\|\tilde{\mathbf{v}} - \mathbf{v}\|_2 \leq \epsilon \|\mathbf{v}\|_2. \quad (3.8)$$

We refer to [21, Section 4.1.1] for more details.

We also consider a dynamic truncation operator \mathbf{T}^{dt} , which is used only for the approximate solution \mathbf{u}_{k+1} . Here a truncated approximation $\tilde{\mathbf{u}}_{k+1}$ of \mathbf{u}_{k+1} is initially computed using block-wise relative truncation

with a prescribed initial tolerance ϵ . Then the algorithm assesses how much the exact solution update $\Delta \mathbf{u}_k = \mathbf{u}_{k+1} - \mathbf{u}_k$ differs from the truncated one $\Delta \tilde{\mathbf{u}}_k = \tilde{\mathbf{u}}_{k+1} - \mathbf{u}_k$ by checking if the condition

$$\left| \frac{\Delta \tilde{\mathbf{u}}_k \cdot \Delta \mathbf{u}_k}{\|\Delta \mathbf{u}_k\|_2^2} - 1 \right| \leq \delta$$

is satisfied, where $\delta > 0$ is a prescribed tolerance. If the condition is satisfied, then $\tilde{\mathbf{u}}_{k+1}$ is accepted as the next iterate. Otherwise, a new tolerance for the relative truncation is selected, equal to $\max\{\alpha\epsilon, \epsilon_{\min}\}$, where $0 < \alpha < 1$ and $\epsilon_{\min} > 0$ is a fixed minimum tolerance. The process is repeated until an acceptable truncated solution is found (or until the tolerance reaches ϵ_{\min}). The final relative tolerance is returned and it is used as initial tolerance for \mathbb{T}^{dt} at the next TPCG iteration. A starting relative tolerance ϵ_0 is fixed at the beginning of the TPCG algorithm. We refer to [21, Section 4.1.2] for more details.

Except for $\tilde{\mathbf{u}}_{k+1}$, all other vectors are compressed using block-wise relative truncation with tolerance

$$\eta_k = \beta \text{tol} \frac{\|\mathbf{r}_0\|_2}{\|\mathbf{r}_k\|_2},$$

where \mathbf{r}_0 and \mathbf{r}_k are the initial and k -th residual vector, respectively, $0 < \beta < 1$ and tol is the TPCG tolerance. This choice of the tolerance promotes low rank, see also [28, 23]. Furthermore, we introduce intermediate truncation steps during the computation of matrix-vector products with \mathbf{A} , motivated by the significant rank increment yielded by this operation. We remark, however, that intermediate truncation can lead to cancellation errors and stagnation, see e.g. the discussion in [29, Section 3.6.3]. Therefore, a strict relative tolerance γ should be chosen to safely perform this step.

The TPCG method is reported in Algorithm 1, while Algorithm 2 and Algorithm 3 perform respectively the matrix-vector products with the system matrix (and possibly the computation of the residual) and the application of the preconditioner. Note that, in the latter algorithms, each vector block is truncated immediately after being computed (for Algorithm 2, this is done in addition to the intermediate truncation steps discussed above).

Remark 1. *If the magnitude of the solution varies significantly in different subdomains, it is a good idea to perform truncations on the vector blocks such that the absolute error (instead of the relative error) is equidistributed. This help in balancing the error among different subdomains. Therefore, given a vector block $\mathbf{y}^{(i,k)}$, belonging to a vector \mathbf{y} , Its truncation $\tilde{\mathbf{y}}^{(i,k)}$ could be chosen by imposing a condition of the form*

$$\|\tilde{\mathbf{y}}^{(i,k)} - \mathbf{y}^{(i,k)}\|_2 \leq \frac{\eta}{\mathcal{N}_{\text{sub}}} \|\mathbf{y}\|_2,$$

for a given $\eta > 0$ independent of $i \in \{1, \dots, \mathcal{N}_{\text{sub}}\}$, and $k \in \{1, 2, 3\}$. Note that in the right-hand side of the above inequality we consider the norm of \mathbf{y} , rather than that of its block $\mathbf{y}^{(i,k)}$.

In the present paper we do not use this strategy since for all problems considered in Section 4, the solution is not significantly larger on a portion of the domain with respect to the rest.

3.4. Subdomains as unions of patches

In the setting described in Section 2.2, we can choose the subdomains as unions of pairs of patches sharing a face. More precisely, for each face shared by two patches, we introduce a subdomain defined as the union of those patches. Note that in this case \mathcal{N}_{sub} is equal to the number of faces belonging to the interface Γ .

We fix $i \in \{1, \dots, \mathcal{N}_{\text{sub}}\}$ and let $i_1, i_2 \in \{1, \dots, \mathcal{N}_{\text{ptc}}\}$ such that $\Theta^{(i)} = \Omega^{(i_1)} \cup \Omega^{(i_2)}$. We assume that if a face of $\Omega^{(i_1)}$ shares an edge with a face of $\Omega^{(i_2)}$, then either both faces belong to $\Gamma \cup \partial\Omega_D$, or they both belong to $\partial\Omega_N$. This assumption guarantees that the space obtained by “merging” $V_{\text{ptc}}^{(i_1)}$ and $V_{\text{ptc}}^{(i_2)}$ can be written as (the pushforward of) a tensor product spline space. Below we give the details.

It is not restrictive to assume that $\Omega^{(i_1)}$ and $\Omega^{(i_2)}$ are attached along the third parametric direction, and in particular that

$$\mathcal{F}_{(i_1)}(\xi_1, \xi_2, 1) = \mathcal{F}_{(i_2)}(\xi_1, \xi_2, 0), \quad (\xi_1, \xi_2) \in [0, 1]^2.$$

Algorithm 1 TPCG

Input: System matrix $\tilde{\mathbf{A}}$ and block diagonal preconditioner $\tilde{\mathbf{P}}$ in block-wise Tucker format, right-hand side $\tilde{\mathbf{f}}$ and initial guess \mathbf{u}_0 in block-wise Tucker format, TPCG tolerance $tol > 0$, parameter β for the relative truncation, intermediate relative truncation tolerance γ , parameters for the dynamic truncation: starting relative tolerance ϵ_0 , reducing factor α , minimum tolerance ϵ_{\min} , threshold δ .

Output: Low-rank solution $\tilde{\mathbf{u}}$ of $\tilde{\mathbf{A}}\tilde{\mathbf{u}} = \tilde{\mathbf{f}}$.

```
1:  $\eta_0 = \beta tol$ ;  
2:  $\mathbf{r}_0 = -\text{Matvec}(\tilde{\mathbf{A}}, \mathbf{u}_0, \tilde{\mathbf{f}}, \eta_0)$   
3:  $\mathbf{z}_0 = \text{Prec}(\tilde{\mathbf{P}}, \mathbf{r}_0, \eta_0)$ ;  
4:  $\mathbf{p}_0 = \mathbf{z}_0$ ;  
5:  $k = 0$   
6: while  $\|\mathbf{r}_k\|_2 > tol$  do  
7:    $\mathbf{q}_k = \text{Matvec}(\tilde{\mathbf{A}}, \mathbf{p}_k, \mathbf{0}, \gamma, \eta_k)$ ;  
8:    $\xi_k = \mathbf{p}_k \cdot \mathbf{q}_k$   
9:    $\omega_k = \frac{\mathbf{r}_k \cdot \mathbf{p}_k}{\xi_k}$ ;  
10:   $[\mathbf{u}_{k+1}, \epsilon_{k+1}] = \text{T}^{\text{dt}}(\mathbf{u}_k, \mathbf{u}_k + \omega_k \mathbf{p}_k, \epsilon_k, \alpha, \epsilon_{\min}, \delta)$ ;  
11:   $\mathbf{r}_{k+1} = -\text{Matvec}(\tilde{\mathbf{A}}, \mathbf{u}_{k+1}, \tilde{\mathbf{f}}, \gamma, \eta_k)$   
12:   $\eta_{k+1} = \beta tol \frac{\|\mathbf{r}_0\|_2}{\|\mathbf{r}_{k+1}\|_2}$ ;  
13:   $\mathbf{z}_{k+1} = \text{Prec}(\mathbf{r}_{k+1}, \eta_{k+1})$ ;  
14:   $\beta_k = -\frac{\mathbf{z}_{k+1} \cdot \mathbf{q}_k}{\xi_k}$ ;  
15:   $\mathbf{p}_{k+1} = \text{T}^{\text{rel}}(\mathbf{z}_{k+1} + \beta_k \mathbf{p}_k, \eta_{k+1})$ ;  
16:   $k = k + 1$ ;  
17: end while  
18:  $\tilde{\mathbf{u}} = \mathbf{u}_k$ .
```

Algorithm 2 Matvec

Input: Matrix $\tilde{\mathbf{A}}$ in block-wise Tucker format, vectors \mathbf{x} and \mathbf{b} in block-wise Tucker format, intermediate and final relative truncation tolerances γ and η

Output: vector $\tilde{\mathbf{y}}$, block-wise truncation of $\mathbf{y} = \tilde{\mathbf{A}}\mathbf{x} - \mathbf{b}$

```
1: for  $i = 1, \dots, \mathcal{N}_{sub}$  do  
2:   for  $k = 1, 2, 3$  do  
3:      $\tilde{\mathbf{y}}^{(i,k)} = -\mathbf{b}^{(i,k)}$   
4:     for  $j = 1, \dots, \mathcal{N}_{sub}$  do  
5:       for  $\ell = 1, 2, 3$  do  
6:          $\tilde{\mathbf{y}}^{(i,k)} = \text{T}^{\text{rel}}\left(\tilde{\mathbf{y}}^{(i,k)} + \tilde{\mathbf{A}}^{(i,j,k,\ell)}\mathbf{x}^{(j,\ell)}, \gamma\right)$   
7:       end for  
8:     end for  
9:      $\tilde{\mathbf{y}}^{(i,k)} = \text{T}^{\text{rel}}\left(\tilde{\mathbf{y}}^{(i,k)}, \eta\right)$   
10:  end for  
11: end for
```

Algorithm 3 Prec

Input: Block diagonal preconditioner $\widetilde{\mathbf{P}}$ with blocks in Tucker format, vector \mathbf{r} in block-wise Tucker format, relative truncation tolerance η

Output: vector $\widetilde{\mathbf{z}}$, block-wise truncation of $\mathbf{z} = \widetilde{\mathbf{P}}^{-1}\mathbf{r}$

```

1: for  $i = 1, \dots, \mathcal{N}_{sub}$  do
2:   for  $k = 1, 2, 3$  do
3:      $\widetilde{\mathbf{z}}^{(i,k)} = \text{Trel} \left( \left( \widetilde{\mathbf{P}}^{(i,k)} \right)^{-1} \mathbf{r}^{(i,k)}, \eta \right)$ 
4:   end for
5: end for

```

Because of the patch conformity assumption, the parametric spline spaces $\widehat{\mathcal{S}}_{ptc}^{(i_1)}$ and $\widehat{\mathcal{S}}_{ptc}^{(i_2)}$ must have the same knot vectors in the first 2 directions, i.e. $\Xi_1^{(i_1)} = \Xi_1^{(i_2)} =: \Xi_1$ and $\Xi_2^{(i_1)} = \Xi_2^{(i_2)} =: \Xi_2$. Moreover, we consider the knot vectors in the third directions

$$\Xi_3^{(i_1)} = \left\{ \underbrace{0, \dots, 0}_{p+1}, \xi_{p+2}^{(i_1)}, \dots, \xi_{m_3^{(i_1)}}^{(i_1)}, \underbrace{1, \dots, 1}_{p+1} \right\}, \quad \Xi_3^{(i_2)} = \left\{ \underbrace{0, \dots, 0}_{p+1}, \xi_{p+2}^{(i_2)}, \dots, \xi_{m_3^{(i_2)}}^{(i_2)}, \underbrace{1, \dots, 1}_{p+1} \right\}.$$

We now define the ‘‘merged’’ spline space $\widehat{\mathcal{S}}_{sub}^{(i)}$, generated by the knot vectors Ξ_1, Ξ_2 and

$$\Xi_3 = \left\{ \underbrace{0, \dots, 0}_{p+1}, \frac{1}{2}\xi_{p+2}^{(i_1)}, \dots, \frac{1}{2}\xi_{m_3^{(i_1)}}^{(i_1)}, \underbrace{\frac{1}{2}, \dots, \frac{1}{2}}_p, \frac{1}{2}\xi_{p+2}^{(i_2)} + \frac{1}{2}, \dots, \frac{1}{2}\xi_{m_3^{(i_2)}}^{(i_2)} + \frac{1}{2}, \underbrace{1, \dots, 1}_{p+1} \right\}.$$

We also consider the geometry mapping $\mathcal{G}_i : [0, 1]^3 \rightarrow \Theta^{(i)}$

$$\mathcal{G}_i(\xi_1, \xi_2, \xi_3) = \begin{cases} \mathcal{F}_{i_1}(\xi_1, \xi_2, 2\xi_3) & \text{if } 0 \leq \xi_3 \leq \frac{1}{2}, \\ \mathcal{F}_{i_2}(\xi_1, \xi_2, 2\xi_3 - 1) & \text{if } \frac{1}{2} < \xi_3 \leq 1. \end{cases} \quad (3.9)$$

We introduce the subspace $\widehat{\mathcal{S}}_{sub,0}^{(j)} \subseteq \widehat{\mathcal{S}}_{sub}^{(j)}$ generated by the basis functions of $\widehat{\mathcal{S}}_{sub}^{(j)}$ whose image through \mathcal{G}_j vanishes on $(\Gamma \setminus (\partial\Omega^{(i_1)} \cap \partial\Omega^{(i_2)})) \cup \partial\Omega_D$. We emphasize that, under the aforementioned assumptions on the boundary conditions, $\widehat{\mathcal{S}}_{sub,0}^{(i)}$ is a tensor product space as in (3.2). It holds

$$V_{sub}^{(i)} = \left\{ \widehat{v}_h \circ \mathcal{G}_i^{-1} \mid \widehat{v}_h \in \widehat{\mathcal{S}}_{sub,0}^{(i)} \right\}.$$

Remark 2. In the case of arbitrary boundary conditions, merging two local spline spaces does not necessarily results in a space which is the pushforward of a tensor product spline space. In this case, one can define $V_{sub}^{(i)}$ by substituting any Neumann boundary conditions with homogenous Dirichlet. Then an additional subdomain should be introduced containing the Neumann degrees of freedom.

We now discuss in detail how the approximations (3.5) and (3.6) can be performed using low-rank techniques. We first consider the case of a matrix block $\mathbf{A}^{(i,j)}$ for $i \neq j$, $i, j \in \{1, \dots, \mathcal{N}_{sub}\}$. Of course if $\Theta^{(i)} \cap \Theta^{(j)}$ has an empty interior, then $\mathbf{A}^{(i,j)}$ is a null matrix. On the other hand, if $\Theta^{(i)} \cap \Theta^{(j)}$ has a non-empty interior, then there is an index $m = m(i, j) \in \{1, \dots, \mathcal{N}_{ptc}\}$ such that $\Theta^{(i)} \cap \Theta^{(j)} = \Omega^{(m)}$. Let $v_h \in V_{sub}^{(i)}$ and $w_h \in V_{sub}^{(j)}$, and let \mathbf{v} and \mathbf{w} be their vector representations. Then for $k, \ell = 1, 2, 3$, it holds

$$\begin{aligned} \mathbf{v}^T \mathbf{A}^{(i,j,k,\ell)} \mathbf{w} &= \int_{\Omega^{(m)}} 2\mu \varepsilon(\underline{e}_k v_h) : \varepsilon(\underline{e}_\ell w_h) + \lambda (\nabla \cdot \underline{e}_k v_h) (\nabla \cdot \underline{e}_\ell w_h) \, d\underline{x} = \\ &= \int_{[0,1]^3} \left(\nabla \widehat{v}_{ptc}^{(m)} \right)^T C^{(m,k,\ell)} \nabla \widehat{w}_{ptc}^{(m)} \, d\underline{\xi}, \end{aligned} \quad (3.10)$$

where $\hat{v}_{ptc}^{(m)} = v_h \circ \mathcal{F}_m$, $\hat{w}_{ptc}^{(m)} = w_h \circ \mathcal{F}_m$, and

$$C^{(m,k,\ell)} = |\det(J_{\mathcal{F}_m})| J_{\mathcal{F}_m}^{-1} [\mu (\delta_{k,\ell} I_3 + \underline{e}_\ell \underline{e}_k^T) + \lambda \underline{e}_k \underline{e}_\ell^T] J_{\mathcal{F}_m}^{-T}.$$

Here $\delta_{k,\ell}$ is the Kronecker delta. Note that $\hat{v}_{ptc}^{(m)}, \hat{w}_{ptc}^{(m)} \in \widehat{\mathcal{S}}_{ptc,0}^{(m)}$. Moreover, if $\text{supp}(v_h) \cap \Omega^{(m)}$ (respectively $\text{supp}(w_h) \cap \Omega^{(m)}$) has an empty interior then $\hat{v}_{ptc}^{(m)}$ (respectively $\hat{w}_{ptc}^{(m)}$) is the null function and $\mathbf{v}^T \mathbf{A}^{(i,j,k,\ell)} \mathbf{w} = 0$.

We consider a low-rank approximation of the entries of $C^{(m,k,\ell)}$:

$$C_{\alpha,\beta}^{(m,k,\ell)}(\xi_1, \xi_2, \xi_3) \approx \sum_{r_1, r_2, r_3} \mathbf{c}_{r_1, r_2, r_3}^{(m,k,\ell,\alpha,\beta)} c_{(1,r_1)}^{(m,k,\ell,\alpha,\beta)}(\xi_1) c_{(2,r_2)}^{(m,k,\ell,\alpha,\beta)}(\xi_2) c_{(3,r_3)}^{(m,k,\ell,\alpha,\beta)}(\xi_3). \quad (3.11)$$

Plugging (3.11) into (3.10), we obtain

$$\mathbf{v}^T \mathbf{A}^{(i,j,k,\ell)} \mathbf{w} \approx \sum_{r_1, r_2, r_3} \sum_{\alpha, \beta=1}^3 \mathbf{c}_{r_1, r_2, r_3}^{(m,k,\ell,\alpha,\beta)} \int_{[0,1]^3} c_{(1,r_1)}^{(m,k,\ell,\alpha,\beta)} c_{(2,r_2)}^{(m,k,\ell,\alpha,\beta)} c_{(3,r_3)}^{(m,k,\ell,\alpha,\beta)} \partial_\alpha \hat{v}_{ptc}^{(m)} \partial_\beta \hat{w}_{ptc}^{(m)} d\xi.$$

Therefore, thanks to the tensor structure of the spline space $\widehat{\mathcal{S}}_{ptc,0}^{(m)}$ the matrix block $\mathbf{A}^{(i,j,k,\ell)}$ can be approximated as

$$\mathbf{A}^{(i,j,k,\ell)} \approx \sum_{r_1, r_2, r_3} \sum_{\alpha, \beta=1}^3 \mathbf{c}_{r_1, r_2, r_3}^{(m,k,\ell,\alpha,\beta)} \tilde{A}_{(3,r_3)}^{(i,j,k,\ell,\alpha,\beta)} \otimes \tilde{A}_{(2,r_2)}^{(i,j,k,\ell,\alpha,\beta)} \otimes \tilde{A}_{(1,r_1)}^{(i,j,k,\ell,\alpha,\beta)}, \quad (3.12)$$

where each Kronecker factor $\tilde{A}_{(d,r_d)}^{(i,j,k,\ell,\alpha,\beta)}$ is an $n_{sub,d}^{(i)} \times n_{sub,d}^{(j)}$ matrix with null entries outside of a square $n_{ptc,d}^{(m)} \times n_{ptc,d}^{(m)}$ block $\tilde{A}_{(d,r_d)}^{(m,k,\ell,\alpha,\beta)}$ whose entries are

$$\left(\tilde{A}_{(d,r_d)}^{(m,k,\ell,\alpha,\beta)} \right)_{s,t} = \int_0^1 c_{(d,r_d)}^{(m,k,\ell,\alpha,\beta)}(\xi_d) \left[\hat{b}_{d,s}^{(m)}(\xi_d) \right]^{(d,\alpha)} \left[\hat{b}_{d,t}^{(m)}(\xi_d) \right]^{(d,\beta)} d\xi_d, \quad s, t = 1, \dots, n_{ptc,d}^{(m)},$$

with

$$[f(\xi)]^{(d,\gamma)} = \begin{cases} f'(\xi) & \text{if } d = \gamma \\ f(\xi) & \text{otherwise} \end{cases}, \quad d, \gamma = 1, 2, 3,$$

Note that (3.12) can be easily written in the Tucker format (3.5).

There is of course more than one approach to compute the low-rank approximation (3.11). A suitable possibility, proposed in [20], is to interpolate the left-hand side function using a coarse spline space and then performing a High Order Singular Value Decomposition (HOSVD) [7]. In this work, however, we follow [21] and employ the strategy described in [9, 8], which is based on interpolation with Chebyshev polynomials.

We now discuss the low-rank approximation of a given vector block $\mathbf{f}^{(i,k)}$, where $i \in \{1, \dots, \mathcal{N}_{ptc}\}$, and $k \in \{1, 2, 3\}$. Let $v_h \in V_{sub}^{(i)}$ and let \mathbf{v} be its vector representation. It holds

$$\mathbf{v}^T \mathbf{f}^{(i,k)} = \int_{\Theta^{(i)}} f_k(\underline{x}) v_h(\underline{x}) d\underline{x} = \int_{[0,1]^3} \hat{f}_k^{(i)}(\underline{\xi}) \hat{v}_{sub}^{(i)}(\underline{\xi}) d\underline{\xi}, \quad (3.13)$$

where $\hat{f}_k^{(i)} = \det(J_{\mathcal{G}_i}) (f_k \circ \mathcal{G}_i^{-1})$ and $\hat{v}_{sub}^{(i)} = v_h \circ \mathcal{G}_i^{-1} \in \widehat{\mathcal{S}}_{sub,0}^{(i)}$. We consider a low-rank approximation

$$\hat{f}_k^{(i)}(\xi_1, \xi_2, \xi_3) \approx \sum_{r_1, r_2, r_3} \mathbf{f}_{r_1, r_2, r_3}^{(i,k)} f_{(1,r_1)}^{(i,k)}(\xi_1) f_{(2,r_2)}^{(i,k)}(\xi_2) f_{(3,r_3)}^{(i,k)}(\xi_3) \quad (3.14)$$

Plugging (3.14) into (3.13) we obtain

$$\mathbf{v}^T \mathbf{f}^{(i,k)} \approx \sum_{r_1, r_2, r_3} \mathbf{f}_{r_1, r_2, r_3}^{(i,k)} \int_{[0,1]^3} f_{(1,r_1)}^{(i,k)}(\xi_1) f_{(2,r_2)}^{(i,k)}(\xi_2) f_{(3,r_3)}^{(i,k)}(\xi_3) \hat{v}_{sub}^{(i)}(\underline{\xi}) d\underline{\xi}.$$

Therefore, thanks to the tensor structure of the spline space $\widehat{\mathcal{S}}_{sub,0}^{(i)}$ the vector block $\mathbf{f}^{(i,k)}$ can be approximated as in (3.6).

We now discuss the technical details of the low-rank approximation (3.14) considered in this work. Assuming that \mathcal{G}_i is given by (3.9), we first use the `Chebfun3F` algorithm [8] to independently compute low-rank approximations of $\hat{f}_k^{(i)} = \det(J_{\mathcal{G}_i})(f_k \circ \mathcal{G}_i^{-1})$ for $0 \leq \xi_3 \leq \frac{1}{2}$ and for $\frac{1}{2} < \xi_3 \leq 1$. The reason for this separation is that $J_{\mathcal{G}_i}$ is possibly discontinuous at $\xi_3 = \frac{1}{2}$ (corresponding to the interface between the two patches in the physical domain) and this could hinder the effectiveness of the considered low-rank Chebyshev approximation. Note that also f_k could be discontinuous. We extend the two approximations of $\hat{f}_k^{(i)}$, denoted with $\tilde{f}_{k,1}^{(i)}$ and $\tilde{f}_{k,2}^{(i)}$, by zero outside of their respective domain. Then we consider

$$\hat{f}_k^{(i)} \approx \tilde{f}_k^{(i)} = \tilde{f}_{k,1}^{(i)} + \tilde{f}_{k,2}^{(i)}.$$

Note that the multilinear rank of $\tilde{f}_k^{(i)}$ is given by the sum of the multilinear ranks of $\tilde{f}_{k,1}^{(i)}$ and $\tilde{f}_{k,2}^{(i)}$. As a final step, we reduce the rank of the approximation using a purely algebraic approach based on the HOSVD.

We finally briefly discuss the Tucker approximation of a given matrix block $\mathbf{A}^{(i,i,k,\ell)}$, where $i \in \{1, \dots, \mathcal{N}_{sub}\}$, $k, \ell \in \{1, 2, 3\}$. Let $v_h, w_h \in V_{sub}^{(i)}$, and let \mathbf{v} and \mathbf{w} be their vector representations. It holds

$$\begin{aligned} \mathbf{v}^T \mathbf{A}^{(i,i,k,\ell)} \mathbf{w} &= \int_{\Theta^{(i)}} 2\mu \varepsilon(\underline{e}_k v_h) : \varepsilon(\underline{e}_\ell w_h) + \lambda (\nabla \cdot \underline{e}_k v_h) (\nabla \cdot \underline{e}_\ell w_h) \, d\underline{x} = \\ &= \int_{[0,1]^3} \left(\nabla \hat{v}_{sub}^{(i)} \right)^T Q^{(i,k,\ell)} \nabla \hat{w}_{sub}^{(i)} \, d\underline{\xi}, \end{aligned} \quad (3.15)$$

where $\hat{v}_{sub}^{(i)} = v_h \circ \mathcal{G}_i$, $\hat{w}_{sub}^{(i)} = w_h \circ \mathcal{G}_i \in \widehat{\mathcal{S}}_{sub,0}^{(i)}$, and

$$Q^{(i,k,\ell)} = |\det(J_{\mathcal{G}_i})| J_{\mathcal{G}_i}^{-1} \left[\mu (\delta_{k,\ell} I_3 + \underline{e}_\ell \underline{e}_k^T) + \lambda \underline{e}_k \underline{e}_\ell^T \right] J_{\mathcal{G}_i}^{-T}.$$

We consider the following low-rank approximations of the entries of $Q^{(i,k,\ell)}$:

$$Q_{\alpha,\beta}^{(i,k,\ell)}(\xi_1, \xi_2, \xi_3) \approx \sum_{r_1, r_2, r_3} \mathbf{q}_{r_1, r_2, r_3}^{(i,k,\ell,\alpha,\beta)} \cdot q_{(1,r_1)}^{(i,k,\ell,\alpha,\beta)}(\xi_1) \cdot q_{(2,r_2)}^{(i,k,\ell,\alpha,\beta)}(\xi_2) \cdot q_{(3,r_3)}^{(i,k,\ell,\alpha,\beta)}(\xi_3). \quad (3.16)$$

This approximation can be computed using the same strategy as for (3.14). Plugging (3.16) into (3.15), and exploiting the tensor structure of $\widehat{\mathcal{S}}_{sub,0}^{(i)}$, we obtain the Tucker approximation (3.5).

Remark 3. *Since the low-rank strategy is meant to effectively tackle large problems, we have considered above the subdomains as union of two adjacent patches. Other strategies are possible, resulting e.g. in a larger number of smaller subdomains. We emphasize that a large number of subdomains would require the introduction of a coarse solver. Indeed, it is well-known that preconditioners based on local domain decomposition without coarse solver are not robust with respect to the number of subdomains.*

4. Numerical experiments

In this section we present some numerical experiments to show the behavior of our low-rank solving strategy for multipatch geometries. All the tests are performed with Matlab R2022b on an Intel(R) Core(TM) i9-12900K, running at 3.20 GHz, and with 128 GB of RAM.

We used GeopDEs toolbox [30] to handle isogeometric discretizations. The approximation of the right-hand side and the linear system matrix are computed using Chebfun toolbox functions [9].

In all the tests, we employ a dyadic refinement and every patch has the same number of elements $n_{el} = 2^L$ in each parametric direction and for different discretization levels L . The numerical solution is computed with the TPCG method, discussed in Section 3.3, with relative tolerance $tol = 10^{-6}$ and the zero vector as initial guess. The system matrix and the right-hand side are approximated with the technique of Section

3.4 by setting the relative tolerance of `Chebfun3F` equal to $10^{-1}tol = 10^{-7}$ (see [8] for more details). The dynamic truncation described in Section 3.3 is used fixing the initial relative tolerance as $\epsilon_0 = 10^{-1}$ and the minimum relative tolerance as $\epsilon_{\min} = tol\|\mathbf{f}\|_2 10^{-1}$. The threshold δ is set equal to 10^{-3} , the reducing factor α is set equal to 0.5. The relative tolerance parameter β is chosen as 10^{-1} , while the intermediate relative tolerance γ is chosen as 10^{-8} . The relative tolerance ϵ_{rel}^{prec} for the approximation of the diagonal blocks of the preconditioner (see [21] for details) is set equal to 10^{-1} . We experimentally verified that these choices of the parameters yield good performance of the TPCG method.

The Lamé parameters are defined as

$$\mu = \frac{E}{2(1+\nu)}, \quad \lambda = \frac{E\nu}{(1+\nu)(1-2\nu)}, \quad (4.1)$$

where E is the Young's modulus and ν the Poisson ratio. Throughout this section, unless otherwise specified, we set $E = 1$ and $\nu = 0.3$.

Let

$$\tilde{\mathbf{u}}^{(j)} := \begin{bmatrix} \tilde{\mathbf{u}}^{(j,1)} \\ \tilde{\mathbf{u}}^{(j,2)} \\ \tilde{\mathbf{u}}^{(j,3)} \end{bmatrix}, \quad j = 1, \dots, \mathcal{N}_{sub}$$

be the solution of the linear elasticity problem in Tucker format in each subdomain. We denote with $(R_1^{\mathbf{u}}(j, d), R_2^{\mathbf{u}}(j, d), R_3^{\mathbf{u}}(j, d))$ the multilinear rank of $\tilde{\mathbf{u}}^{(j,d)}$, for $d = 1, 2, 3$ and $j = 1, \dots, \mathcal{N}_{sub}$. The memory requirements in percentage of the low-rank solution with respect to the full solution is defined as

$$\text{memory requirements in \%} := \frac{\sum_{j=1}^{\mathcal{N}_{sub}} \sum_{d=1}^3 \left(R_1^{\mathbf{u}}(j, d)n_{sub,1}^{(j)} + R_2^{\mathbf{u}}(j, d)n_{sub,2}^{(j)} + R_3^{\mathbf{u}}(j, d)n_{sub,3}^{(j)} \right)}{N_{dof}} \cdot 100, \quad (4.2)$$

where $N_{dof} := \sum_{j=1}^{\mathcal{N}_{sub}} n_{sub,1}^{(j)} n_{sub,2}^{(j)} n_{sub,3}^{(j)}$ represents the total number of degrees of freedom, i.e. the dimension of the space $\sum_{j=1}^{\mathcal{N}_{sub}} V_{sub}^{(j)}$. Note that we only consider the memory compression of the solution and not the memory compression of the right-hand side and of the linear system matrix, that has already been analyzed in [20, 13, 3].

In the numerical experiments we show the maximum of the multilinear rank of all the components of the solution. Thanks to the strategy employed for the truncation of the iterates $\mathbf{r}_k, \mathbf{z}_k, \mathbf{p}_k$ and \mathbf{q}_k , the maxima of their multilinear ranks is comparable to the one of \mathbf{u}_k when convergence approaches, and thus their values are not reported.

Perhaps not surprisingly, our numerical experience indicates that the main effort of the TPCG iteration in terms of computation time is represented by the truncation steps. Anyway, since our Matlab implementation is not optimized, we prefer not to report a complete distribution of the computation time throughout the algorithm.

4.1. L-shaped domain

In this test we consider a three dimensional L-shaped domain, as represented in Figure 2a, where different colors represent different patches. We have two subdomains, one is the union of the yellow and light green patches and the other the union of the light green and dark green patches.

For this domain, we preliminary perform a convergence test to assess that the numerical solution yielded by our approach is indeed a good approximation of the Galerkin solution. For this purpose, we consider a Poisson toy problem with homogeneous Dirichlet boundary conditions and source function $f(x, y, z) = \sin(2\pi x) \sin(2\pi y) \sin(2\pi z)$. Note that the exact solution of this toy problem is $u(x, y, z) = - (12\pi^2)^{-1} f(x, y, z)$. We assemble and solve the problem with a low-rank strategy analogous to that described previously (in particular we fix 10^{-10} as tolerance for TPCG) and then compute the H^1 and L^2 norms of the error for the obtained solution, for different discretization levels and polynomial degrees. Results are shown in Figure 1 and confirm the validity of our approach.

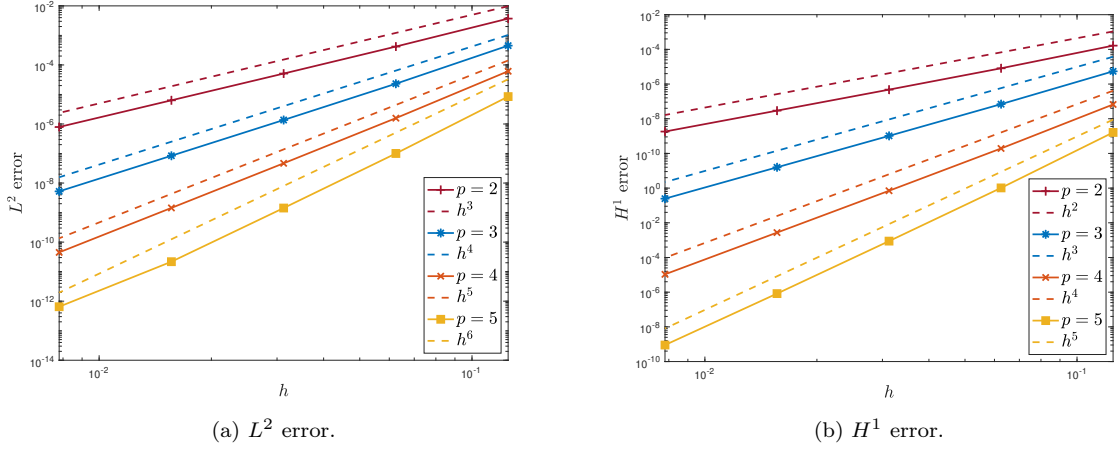


Figure 1: Errors for a Poisson problem in the L-shaped domain.

We now solve a linear elasticity problem on the same domain, we set the right-hand side equal to $\underline{f} = [0, 0, -0.3]^T$ and we consider homogeneous Dirichlet boundary conditions on the patch faces that lie on the planes $\{x = -1\} \cup \{z = 1\} \cup \{x = 0\} \cup \{z = 0\}$, and homogeneous Neumann boundary conditions elsewhere. The numerical solution is represented in Figure 2b.

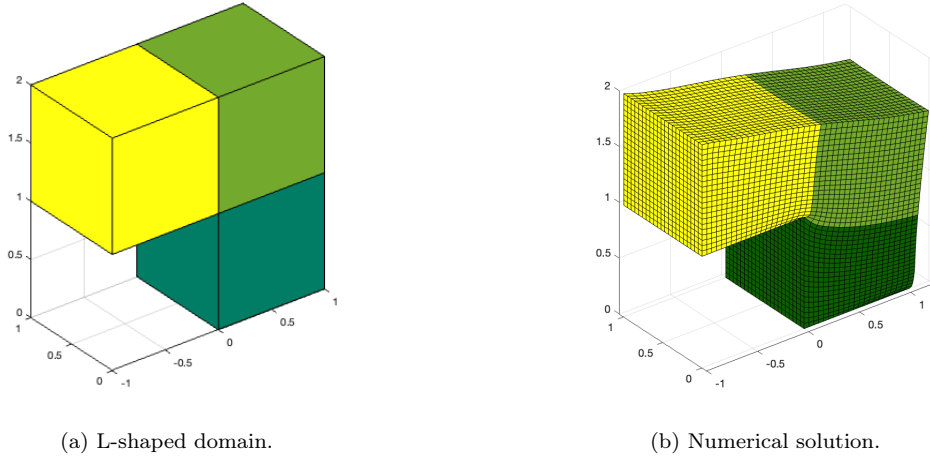


Figure 2: Initial geometry and numerical solution for the L-shaped domain.

For this domain, the multilinear ranks of the blocks of $\tilde{\mathbf{A}}$ (note that here the geometry is trivial for all patches, therefore $\mathbf{A} = \tilde{\mathbf{A}}$) are

$$(R_1^A(i, j, k, k), R_2^A(i, j, k, k), R_3^A(i, j, k, k)) = (3, 3, 3), \quad k = 1, 2, 3,$$

and

$$(R_1^A(i, j, k, \ell), R_2^A(i, j, k, \ell), R_3^A(i, j, k, \ell)) = (2, 2, 2), \quad k, \ell = 1, 2, 3, k \neq \ell,$$

for $i, j = 1, 2$.

In Table 1 we report the number of iterations for degrees $p = 2, 3, 4, 5$ and number of elements per patch per parametric direction $n_{el} = 2^L$ with $L = 5, 6, 7, 8$. The number of iterations is almost independent of the

degree and grows only mildly with the number of elements n_{el} . We emphasize that for the finer discretization level the number of degrees of freedom is roughly 200 millions.

n_{el}	Iteration number			
	$p = 2$	$p = 3$	$p = 4$	$p = 5$
32	34	36	34	35
64	37	38	36	37
128	43	42	40	41
256	52	51	48	49

Table 1: Number of iterations for the L-shaped domain.

Figure 3a shows the maximum of the multilinear ranks of the solution in all the displacement directions and in all the subdomains: the ranks grow as the degree and number of elements is increased, implying that the solution has not a low rank. The memory compression (4.2), represented in Figure 3b, highlights the great memory saving that we have with the multipatch low-rank strategy with respect to the full one. Note that the maximum rank of the solution is rather large, between 100 and 150 on the finest discretization level. Nevertheless, the memory compression is around 1% for this level.

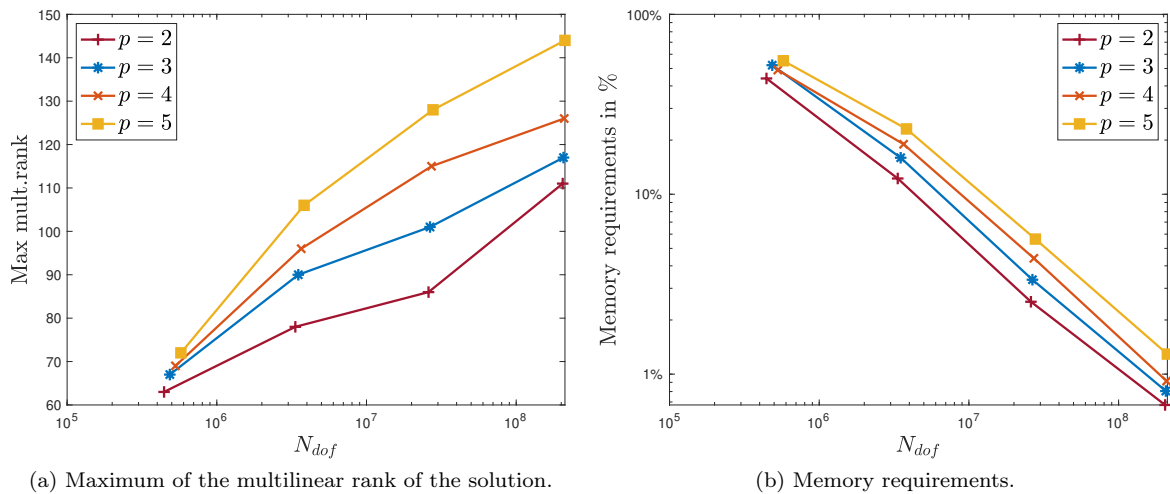


Figure 3: Results for the L-shaped domain.

4.2. 3D-cross domain

In this test, we consider a 3D-cross domain, as represented in Figure 4a. Note that in this domain we have that the central cube belongs to six subdomains, which is the maximum allowed by our strategy. We consider homogeneous Dirichlet boundary conditions everywhere, except for the external faces, and right-hand side equal to $\underline{f} = [0, 0, -2]^T$. The numerical solution is represented in Figure 4b. The multilinear ranks of the blocks of $\tilde{\mathbf{A}}$ are

$$(R_1^A(i, j, k, k), R_2^A(i, j, k, k), R_3^A(i, j, k, k)) = (3, 3, 3), \quad k = 1, 2, 3,$$

and

$$(R_1^A(i, j, k, \ell), R_2^A(i, j, k, \ell), R_3^A(i, j, k, \ell)) = (2, 2, 2), \quad k, \ell = 1, 2, 3, k \neq \ell,$$

for $i, j = 1, \dots, 6$.

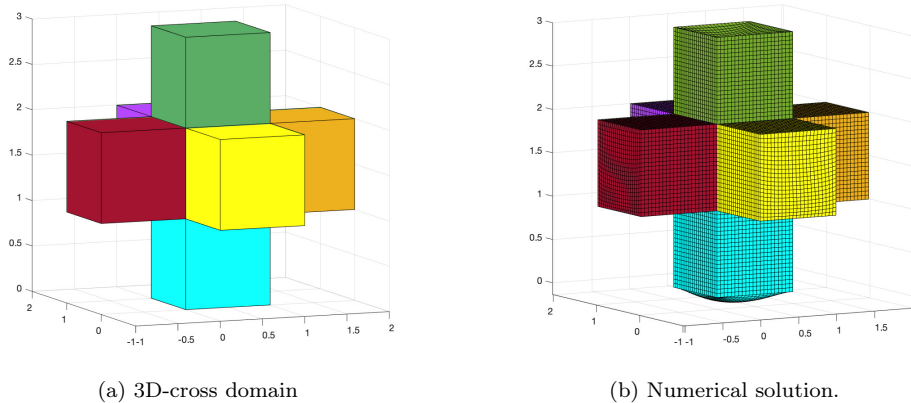


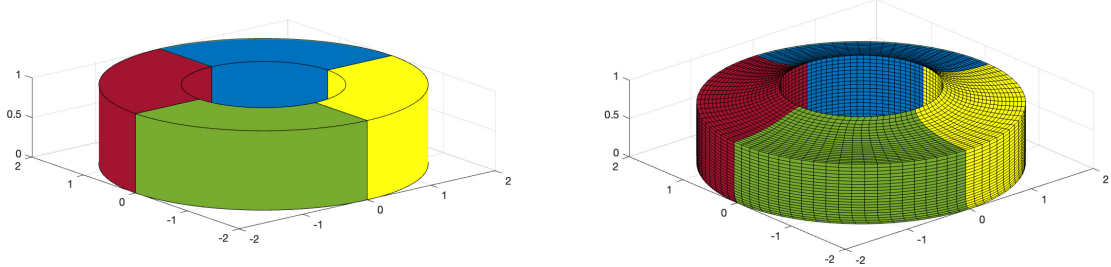
Figure 4: Initial geometry and numerical solution for the 3D-cross domain.

The number of iterations for degrees $p = 2, 3, 4, 5$ and number of elements per parametric direction $n_{el} = 2^L$ with $L = 5, 6, 7, 8$ is reported in Table 2. The number of iterations is almost independent on the degree and mesh-size. These numbers are similar, although slightly higher, to the ones of Table 1 relative to the L-shaped domain: the proposed low-rank strategy seems to be independent on the number of subdomains to which a patch belongs.

	Iteration number			
	$p = 2$	$p = 3$	$p = 4$	$p = 5$
$n_{el} = 32$	49	51	51	50
$n_{el} = 64$	50	54	52	51
$n_{el} = 128$	51	53	54	53
$n_{el} = 256$	55	57	57	57

Table 2: Number of iterations for the cross domain.

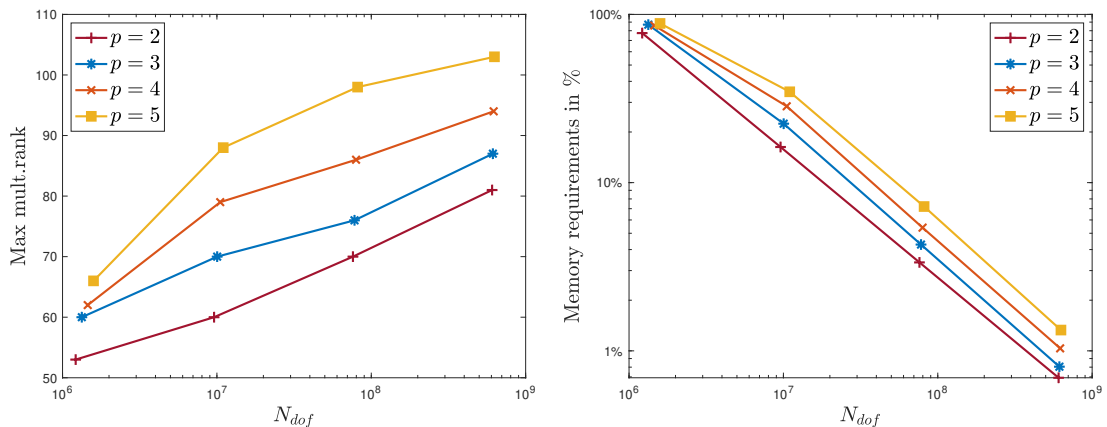
We report in Figure 5a the maximum of the multilinear ranks of the solution in all the directions and for all the subdomains. The multilinear rank of the solution increases with the number of elements per direction n_{el} . However, the memory storage for the solution is hugely reduced with respect to the full solution and reaches values around 1% for the highest discretization level, as represented in Figure 5b.



(a) Ring domain.

(b) Numerical solution.

Figure 6: Initial geometry and numerical solution for the ring domain.



(a) Maximum of the multilinear rank of the solution.

(b) Memory requirements.

Figure 5: Results for the 3D-cross domain.

4.3. Ring domain

In this test we consider a thick ring domain, represented in Figure 6a. We have four patches and four subdomains, represented by the union of green and yellow patches, yellow and blue patches, blue and red patches and red and green patches. We impose homogeneous Dirichlet boundary conditions on $\{z = 0\}$ and in the central walls of the ring, while homogeneous Neumann boundary conditions are imposed elsewhere. We set the right-hand side equal to $\underline{f} = [0, 0, -0.5]^T$. The numerical solution is represented in Figure 6b.

For this domain, the multilinear ranks of the blocks of $\tilde{\mathbf{A}}$ are

$$(R_1^A(i, j, 1, 1), R_2^A(i, j, 1, 1), R_3^A(i, j, 1, 1)) = (R_1^A(i, j, 2, 2), R_2^A(i, j, 1, 1), R_3^A(i, j, 2, 2)) = (5, 5, 5),$$

$$(R_1^A(i, j, 3, 3), R_2^A(i, j, 3, 3), R_3^A(i, j, 3, 3)) = (3, 3, 3)$$

and

$$(R_1^A(i, j, k, \ell), R_2^A(i, j, k, \ell), R_3^A(i, j, k, \ell)) = (4, 4, 4), \quad k, \ell = 1, 2, 3, k \neq \ell,$$

for $i, j = 1, 2, 3, 4$ s.t. $\Theta^{(i)} \cap \Theta^{(j)}$ has non-zero measure.

Table 3 collects the number of iterations for degrees $p = 2, 3, 4, 5$ and number of elements per patch per parametric direction $n_{el} = 2^L$ with $L = 5, 6, 7, 8$, as in the previous test. The number of iterations is independent of the meshsize h and appears to be stable with respect to the polynomial degree p , although the case $p = 2$ shows higher iteration counts compared to the higher degrees.

n_{el}	Iteration number			
	$p = 2$	$p = 3$	$p = 4$	$p = 5$
32	59	42	39	40
64	63	44	41	42
128	71	50	46	46
256	77	60	58	55

Table 3: Number of iterations for the ring domain.

We report in Figure 7a the maximum of the multilinear ranks of the solution in all the directions and for all the subdomains. Interestingly, for degrees 2 and 4 this maximum rank appears to grow in the left part of the plot (corresponding to small values of n_{el}), but it then decreases as n_{el} grows and on the finest discretization level in both cases it reaches a value between 60 and 70, which is also (roughly) the maximum rank observed for degree 3.

Nevertheless, as represented in Figure 7b, the memory storage for the solution is hugely reduced with respect to the full solution and reaches values around 1% for the highest discretization level.

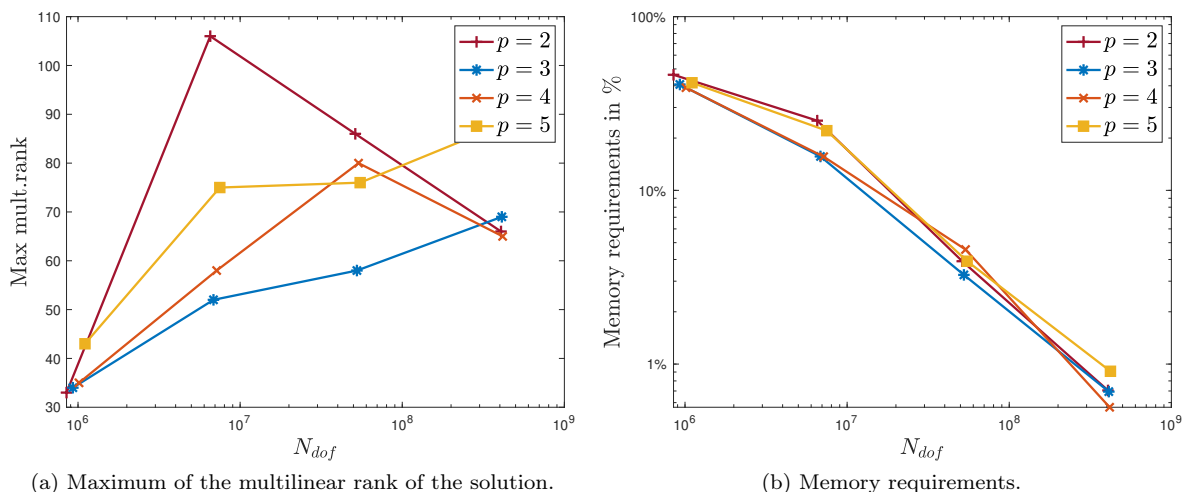


Figure 7: Results for the ring domain.

We perform an additional test using the same geometry, boundary conditions and forcing term, considering non-constant Lamé parameters. In particular, in (4.1) we set $\nu = 0.3$ and $E = 1 + \frac{1 + \sin(\theta(x, y))}{2}$, where $\theta(x, y)$ is the argument of the complex number $x + iy$. The numerical solution is represented in Figure 8.

The numbers of TPCG iterations are reported in Table 4, while the maxima of the multilinear ranks of the solution and memory requirements are shown in Figure 9, for different different degrees and numbers of elements. The results are similar to the case with constant parameters.

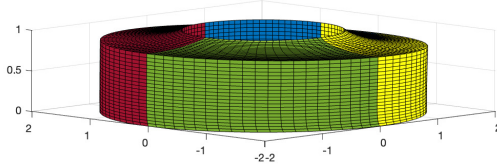


Figure 8: Numerical solution for the ring domain (variable Lamé parameters).

n_{el}	Iteration number			
	$p = 2$	$p = 3$	$p = 4$	$p = 5$
32	71	46	43	45
64	77	48	45	47
128	84	53	51	51
256	96	70	65	65

Table 4: Number of iterations for the ring domain (variable Lamé parameters).

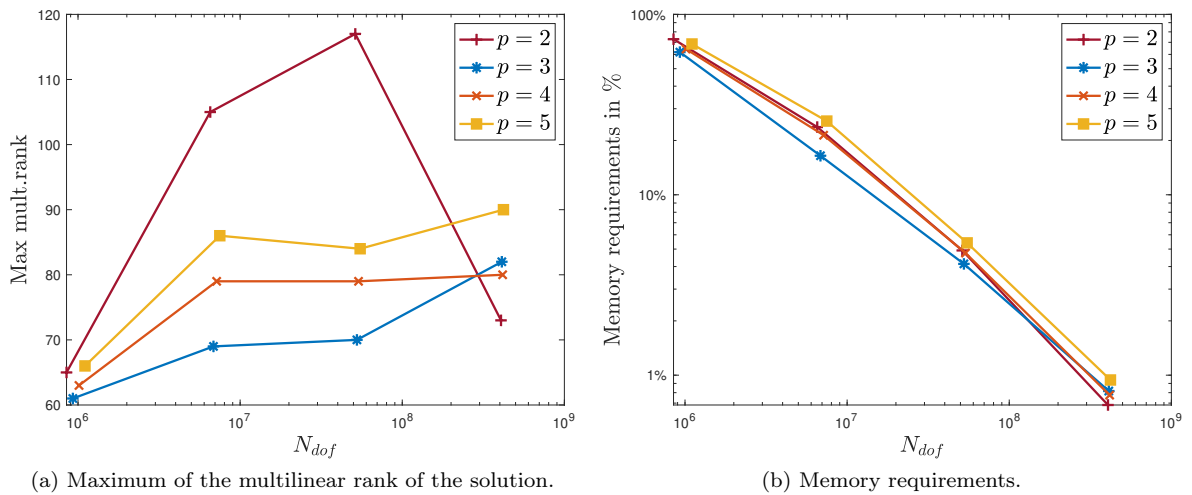


Figure 9: Results for the ring domain (variable Lamé parameters).

4.4. Igloo-shaped domain

In this test we consider an igloo-shaped domain, represented in Figure 10a. As in the previous test case, we have four patches and four subdomains, represented by the union of green and yellow patches, yellow and

blue patches, blue and red patches and red and green patches. We impose homogeneous Dirichlet boundary conditions on $\{z = 0\}$ and the internal boundary, while homogeneous Neumann boundary conditions are imposed elsewhere. We set the right-hand side equal to $\underline{f} = [0, 0, -1]^T$. The numerical solution is represented in Figure 10b.

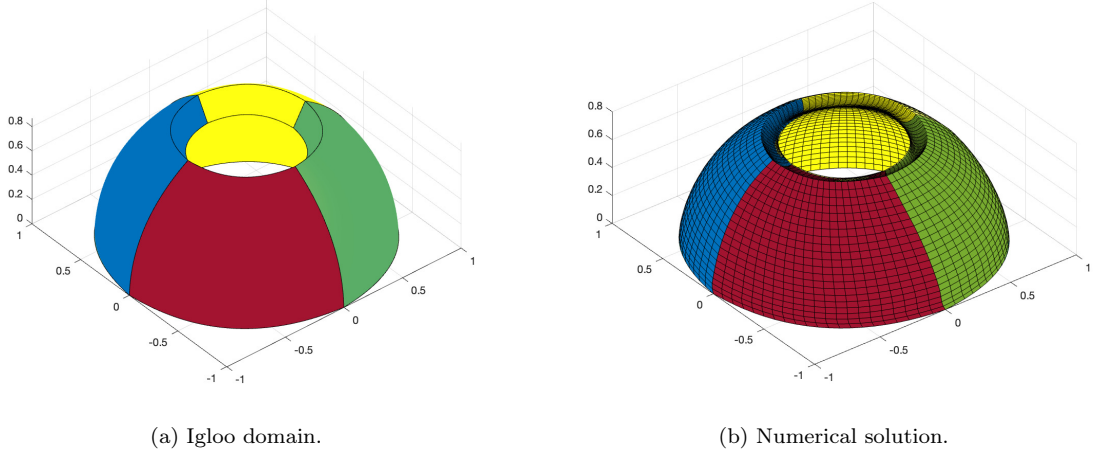


Figure 10: Initial geometry and numerical solution for the igloo-shaped domain.

The multilinear ranks of the blocks of $\tilde{\mathbf{A}}$ are

$$(R_1^A(i, j, 1, 1), R_2^A(i, j, 1, 1), R_3^A(i, j, 1, 1)) = (R_1^A(i, j, 2, 2), R_2^A(i, j, 1, 1), R_3^A(i, j, 2, 2)) = (13, 13, 9),$$

for $i, j = 1, \dots, 4$ s.t. $\Theta^{(i)} \cap \Theta^{(j)}$ has zero measure, while

$$(R_1^A(i, i, 3, 3), R_2^A(i, i, 3, 3), R_3^A(i, i, 3, 3)) = (13, 13, 9) \quad \text{for } i = 1, \dots, 4$$

$$(R_1^A(i, j, 3, 3), R_2^A(i, j, 3, 3), R_3^A(i, j, 3, 3)) = (12, 12, 9) \quad \text{for } i \neq j \text{ and } i, j = 1, \dots, 4,$$

s.t. $\Theta^{(i)} \cap \Theta^{(j)}$ has non-zero measure. Finally,

$$(R_1^A(i, j, k, l), R_2^A(i, j, k, l), R_3^A(i, j, k, l)) = (9, 9, 9), \quad \text{if } (k, l) \in \{(1, 2), (2, 1)\},$$

and

$$(R_1^A(i, j, k, l), R_2^A(i, j, k, l), R_3^A(i, j, k, l)) = (8, 8, 8), \quad \text{if } (k, l) \in \{(1, 3), (3, 1), (2, 3), (3, 2)\}$$

for $i, j = 1, \dots, 4$ s.t. $\Theta^{(i)} \cap \Theta^{(j)}$ has zero measure. Indeed, in Table 5 we reported the number of iterations for degrees $p = 2, 3, 4$ and a number of elements per parametric direction $n_{el} = 2^L$ with $L = 4, 5, 6$. Note that the maximum values of L and p is slightly smaller than in the two previous tests. This is due to the higher multilinear ranks of this geometry. Nevertheless, note that the number of degrees of freedom for the finest discretizations level is higher than 7 millions.

n_{el}	Iteration number		
	$p = 2$	$p = 3$	$p = 4$
16	78	49	45
32	87	52	51
64	98	59	58

Table 5: Number of iterations for the igloo-shaped domain.

The maximum of the multilinear ranks of the solution in all the directions and for all the subdomains are represented in Figure 11a.

The gain in terms of storage may seem less significant than in the previous cases, but it is in fact very similar if the comparison is done for the same discretization level. For this problem, on the finest discretization level, the memory storage of the low-rank solution is less than 35% that of the full solution.

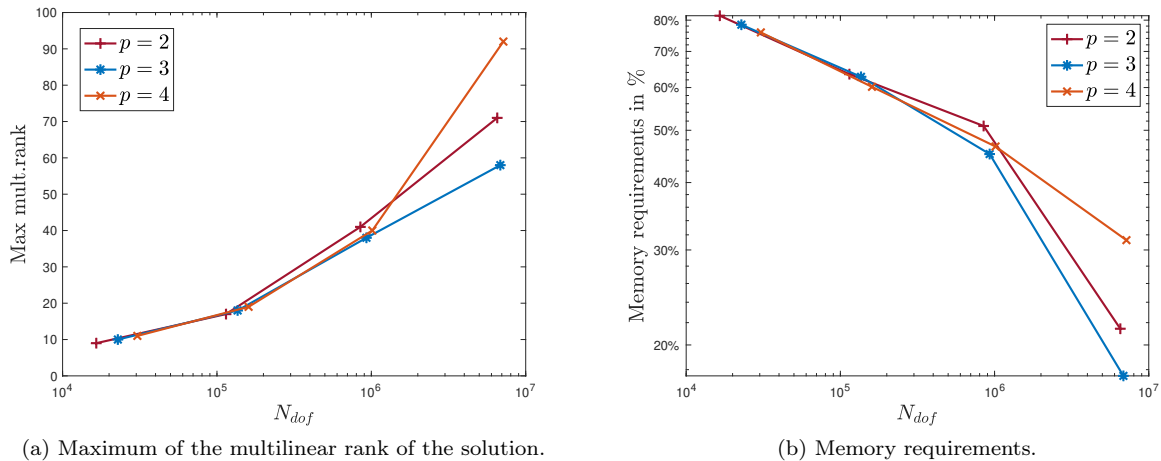


Figure 11: Results for the igloo domain.

5. Conclusions

In this work, we have considered the isogeometric discretization of a compressible linear elasticity problem. We have extended the low-rank solution method presented [21], which is based on a low-rank Tucker representation of vectors and matrices, to conforming multipatch discretizations. This solver exploits the domain decomposition paradigm, where the subdomains are built from union of pairs of adjoining patches. Each block of the system matrix and each block of the right hand side vector is approximated by a Tucker matrix and a Tucker vector, respectively. The resulting linear system is solved by a truncated preconditioned conjugate gradient method. The designed preconditioner has a block-diagonal structure where each block is a Tucker matrix and its application exploits the fast diagonalization method and the fast Fourier transform.

We performed numerical tests assessing a low memory storage, almost independent of the degree p , and the number of iterations independent of p and the mesh-size.

The problems considered are simple academic benchmarks, and we emphasize that the effectiveness of these techniques is greater when the rank of the considered approximation of the problem's components (the geometry, the operator coefficients, the forcing term, and therefore the solution) is lower. The promising results obtained suggest further exploring, in future work, the potential of the proposed method in realistic

applications. The method relies on the linearity of the problem, however, nonlinear problems could be addressed by combining outer Newton-type solvers with inner solvers of the proposed type for the linearized step.

Our tests also demonstrate that our procedure achieves the optimal accuracy expected by the isogeometric scheme. However, this paper does not delve into the theoretical error study. Beyond the convergence theory of truncated iterative solvers, which is a significant open research area, there is also the fundamental issue of understanding how the low-rank approximation of the problem and the subsequent approximations introduced by the solver impact the accuracy of the numerical solution. This study is non-trivial, given that low-rank truncations are computed measuring the approximation w.r.t. the euclidean norms, which is not the natural norm for the well-posedness of the (discretized) differential equation. The topic warrants further investigation and will be the focus of future research.

Acknowledgments

The authors are members of the Gruppo Nazionale Calcolo Scientifico-Istituto Nazionale di Alta Matematica (GNCS-INDAM), the first author was partially supported by INDAM-GNCS Project “Sviluppo di metodi numerici innovativi ed efficienti per la risoluzione di PDE”, while the third author was partially supported by INDAM-GNCS Project “Nodi, ascisse e punti: scegliere e usare in maniera efficiente”. The second author acknowledges support from PNRR-M4C2-I1.4-NC-HPC-Spoke6. The third author acknowledges the contribution of the Italian Ministry of University and Research (MUR) through the PRIN project COSMIC (No. 2022A79M75). The second and the third author acknowledge support from the PRIN 2022 PNRR project NOTES (No. P2022NC97R).

References

- [1] A. Bressan, M. Martinelli, and G. Sangalli. Overlapping subspaces and singular systems with application to isogeometric analysis. Technical report, <https://doi.org/10.48550/arXiv.2408.17273>, 2024.
- [2] A. Bressan and E. Sande. Approximation in FEM, DG and IGA: a theoretical comparison. *Numerische Mathematik*, 143:923–942, 2019.
- [3] A. Bünger, S. Dolgov, and M. Stoll. A low-rank tensor method for PDE-constrained optimization with isogeometric analysis. *SIAM Journal on Scientific Computing*, 42(1):A140–A161, 2020.
- [4] A. Bünger, T.-C. Riemer, and M. Stoll. IETI-based low-rank method for PDE-constrained optimization. *arXiv preprint arXiv:2405.06458*, 2024.
- [5] J. A. Cottrell, T. J. R. Hughes, and Y. Bazilevs. *Isogeometric analysis: toward integration of CAD and FEA*. John Wiley & Sons, 2009.
- [6] C. De Boor. *A practical guide to splines (revised edition)*. Applied Mathematical Sciences. Springer, 2001.
- [7] L. De Lathauwer, B. De Moor, and J. Vandewalle. A multilinear singular value decomposition. *SIAM journal on Matrix Analysis and Applications*, 21(4):1253–1278, 2000.
- [8] S. Dolgov, D. Kressner, and C. Strossner. Functional Tucker approximation using Chebyshev interpolation. *SIAM Journal on Scientific Computing*, 43(3):A2190–A2210, 2021.
- [9] T. A. Driscoll, N. Hale, and L. N. Trefethen. *Chebfun Guide*. Pafnuty Publications, 2014.
- [10] J. A. Evans, Y. Bazilevs, I. Babuška, and T. J. R. Hughes. n -widths, sup-infs, and optimality ratios for the k -version of the isogeometric finite element method. *Computer Methods in Applied Mechanics and Engineering*, 198:1726–1741, 2009.
- [11] J. C. Fuentes, T. Elguedj, D. Dureisseix, and A. Duval. A cheap preconditioner based on fast diagonalization method for matrix-free weighted-quadrature isogeometric analysis applied to nonlinear transient heat transfer problems. *Computer Methods in Applied Mechanics and Engineering*, 414:116157, 2023.
- [12] I. Georgieva and C. Hofreither. Greedy low-rank approximation in Tucker format of solutions of tensor linear systems. *Journal of Computational and Applied Mathematics*, 358:206–220, 2019.
- [13] C. Hofreither. A black-box low-rank approximation algorithm for fast matrix assembly in isogeometric analysis. *Computer Methods in Applied Mechanics and Engineering*, 333:311–330, 2018.
- [14] T. J. R. Hughes, J. A. Cottrell, and Y. Bazilevs. Isogeometric analysis: Cad, finite elements, nurbs, exact geometry and mesh refinement. *Computer methods in applied mechanics and engineering*, 194(39-41):4135–4195, 2005.
- [15] I. C. F. Ipsen and C. D. Meyer. The idea behind krylov methods. *The American mathematical monthly*, 105(10):889–899, 1998.
- [16] B. Jüttler and D. Mokrš. Low rank interpolation of boundary spline curves. *Computer Aided Geometric Design*, 55:48–68, 2017.
- [17] E. F. Kaasschieter. Preconditioned conjugate gradients for solving singular systems. *Journal of Computational and Applied mathematics*, 24(1-2):265–275, 1988.

- [18] D. Kressner and C. Tobler. Low-rank tensor Krylov subspace methods for parametrized linear systems. *SIAM Journal on Matrix Analysis and Applications*, 32(4):1288–1316, 2011.
- [19] R. E. Lynch, J. R. Rice, and D. H. Thomas. Direct solution of partial difference equations by tensor product methods. *Numerische Mathematik*, 6(1):185–199, 1964.
- [20] A. Mantzaflaris, B. Jüttler, B. N. Khoromskij, and U. Langer. Low rank tensor methods in Galerkin-based isogeometric analysis. *Comput. Methods Appl. Mech. Engrg.*, 316:1062–1085, 2017.
- [21] M. Montardini, G. Sangalli, and M. Tani. A low-rank isogeometric solver based on tucker tensors. *Computer Methods in Applied Mechanics and Engineering*, 417:116472, 2023.
- [22] I. V. Oseledets, D. V. Savostyanov, and E. E. Tyrtyshnikov. Linear algebra for tensor problems. *Computing*, 85(3):169–188, 2009.
- [23] D. Palitta and P. Kürschner. On the convergence of Krylov methods with low-rank truncations. *Numerical Algorithms*, 88(3):1383–1417, 2021.
- [24] M. Pan and F. Chen. Low-rank parameterization of volumetric domains for isogeometric analysis. *Computer-Aided Design*, 114:82–90, 2019.
- [25] L. Reichel and Q. Ye. Breakdown-free GMRES for singular systems. *SIAM Journal on Matrix Analysis and Applications*, 26(4):1001–1021, 2005.
- [26] G. Sangalli and M. Tani. Isogeometric preconditioners based on fast solvers for the Sylvester equation. *SIAM Journal on Scientific Computing*, 38(6):A3644–A3671, 2016.
- [27] V. Simoncini and Y. Hao. Analysis of the truncated conjugate gradient method for linear matrix equations. *SIAM Journal on Matrix Analysis and Applications*, 44(1):359–381, 2023.
- [28] V. Simoncini and D. B. Szyld. Theory of inexact Krylov subspace methods and applications to scientific computing. *SIAM Journal on Scientific Computing*, 25(2):454–477, 2003.
- [29] C. Tobler. *Low-rank tensor methods for linear systems and eigenvalue problems*. PhD thesis, ETH Zurich, 2012.
- [30] R. Vázquez. A new design for the implementation of isogeometric analysis in Octave and Matlab: GeoPDEs 3.0. *Computers & Mathematics with Applications*, 72(3):523–554, 2016.